EFFECT OF GOLD NANOROD PROPERTIES ON LSPR RESPONSE

A Thesis Submitted to
the Graduate School of
Izmir Institute of Technology
in Partial Fulfillment of the Requirements for the Degree of

MASTER OF SCIENCE

in Biotechnology

by
Şebnem KILIÇ

July 2023
İZMİR

We approve the thesis of **Şebnem KILIÇ**

Examining Committee Members:

Prof. Dr. Volga BULMUŞ

Bioengineering, İzmir Institute of Technology

Asst. Prof. Dr. Hümeyra TAŞKENT SEZGİN

Bioengineering, İzmir Institute of Technology

Asst. Prof. Dr. Gizem KALELİ CAN

Biomedical Engineering, Izmir Democracy University

19 July 2023

Prof. Dr. Volga BULMUŞ

Supervisor, Bioengineering,

İzmir Institute of Technology

Assoc.Prof. Hüseyin Cumhur TEKİN

Co-Supervisor, Bioengineering,

İzmir Institute of Technology

Doç. Dr. Ali Oğuz BÜYÜKKİLECİ

Head of the Department of Biotechnology

Prof. Dr. Mehtap EANES

Dean of the Graduate School of Education

ACKNOWLEDGMENTS

I would like to start by thanking my advisor, Prof. Dr. Volga BULMUŞ, for getting me interested in my project and helping me every step of the way. Her determination, knowledge, and helpful suggestions helped a lot in getting this job done. Also, I'd like to thank Associate Professor Dr. Hüseyin Cumhur TEKİN, who is my co-advisor.

I also want to express my gratitude to the Department of Biotechnology and Bioengineering's faculty for helping me with my research. Through the classes and seminar I took as part of their curriculum, they assisted me in expanding my knowledge.

A special thanks goes out to the integrated research center, which was instrumental in making this study a reality. I was able to complete the data collection and analysis procedure because of their facilities and resources.

Additionally, I want to thank my family for their support in helping me complete this thesis, as well as my lab mates, roommate Fatma Defne ÇALIK, and other close friends Nazrin Mammadzadaa and Mustafa Bahreldeen Hamed Nour. This thesis would not have been possible without their ongoing encouragement and emotional support.

ABSTRACT

EFFECT OF GOLD NANOROD PROPERTIES ON LSPR RESPONSE

Optical qualities make gold nanorods (GNRs) excellent for plasmonic biosensors. Localized surface plasmon resonance (LSPR) phenomenon which occurs on GNR surfaces enables the creation of highly sensitive biosensors. The physical properties such as aspect ratio and size are directly related to the LSPR response of GNRs.

The aim of this study is to investigate the impact of the aspect ratio (AR) and the interparticle distance on the localized surface plasmon resonance (LSPR) response of GNRs decorated glass sensor chips. For this aim, GNRs were first synthesized using a seed-mediated growth method. The effect of $AgNO_3$ concentration on the AR of GNRs was investigated. It was observed that increasing $AgNO_3$ concentration resulted in GNRs with higher AR and a red shift in the longitudinal plasmon peak wavelength. GNRs with an AR of 4, 6 and 8 were successfully synthesized. Next, the effect of the stabilizer molecule type and molecular weight on the distribution of GNRs on the silanized glass surface was investigated. It was found that the APTES modified glass surfaces cannot be coated with CTAB stabilized GNRs. Using GNRs stabilized with PEG5K resulted in a more homogeneous distribution of GNRs on the glass surface with respect to GNRs stabilized with PEG2K. The interparticle distance between GNRs on the glass surface was successfully controlled by simply concentrating or diluting the GNR solution used for coating the glass surfaces. It was observed that the LSPR peak shifts decreased upon binding of analytes as the interparticle distance between GNRs decreased in the studied range. On the other hand, as the AR decreased, the LSPR response of the GNRs shifted blue. The results presented in this thesis may contribute to future research to improve the potential of LSPR-based biosensors for diverse biomedical and diagnostic applications.

ÖZET

ALTIN NANOROD ÖZELLİKLERİNİN LSPR CEVABINA ETKİSİ

Optik kaliteler, altın nanoçubukları (GNR'ler) plazmonik biyosensörler için mükemmel kılar. GNR yüzeylerinde meydana gelen lokalize yüzey plazmon rezonans (LSPR) olgusu, oldukça hassas biyosensörlerin oluşturulmasını sağlar. En boy oranı ve boyut gibi fiziksel özellikler, GNR'lerin LSPR yanıtıyla doğrudan ilişkilidir.

Bu çalışmanın amacı, GNR'lerin en-boy oranının (AR) ve parçacıklar arası mesafesinin, GNR'lerle dekore edilmiş cam sensör çiplerinin lokalize yüzey plazmon rezonansı (LSPR) tepkisi üzerindeki etkisini araştırmaktır. Bu amaçla, GNR'ler ilk önce tohum aracılı bir büyüme yöntemi kullanılarak sentezlendi. AgNO3 konsantrasyonunun GNR'lerin AR'si üzerindeki etkisi araştırıldı. Artan AgNO3 konsantrasyonunun, daha yüksek AR'li GNR'lere ve uzunlamasına plazmon pik dalga boyunda kırmızıya kaymaya neden olduğu gözlendi. AR değeri 4, 6 ve 8 olan GNR'ler başarıyla sentezlendi. Daha sonra, dengeleyici molekül tipinin ve molekül ağırlığının silanize cam yüzey üzerindeki GNR'lerin dağılımı üzerindeki etkisi araştırıldı. APTES ile modifiye edilmiş cam yüzeylerin CTAB ile stabilize edilmiş GNR'ler ile kaplanamadığı görülmüştür. PEG5K ile stabilize edilmiş GNR'lerin kullanılması, PEG2K ile stabilize edilmiş GNR'lere göre cam yüzeyinde GNR'lerin daha homojen bir şekilde dağılmasına neden olmuştur. Cam yüzeyindeki GNR'ler arasındaki parçacıklar arası mesafe, cam yüzeyleri kaplamak için kullanılan GNR çözeltisinin basitçe konsantre edilmesi veya seyreltilmesiyle başarılı bir şekilde kontrol edildi. Çalışılan aralıkta GNR'ler arasındaki parçacıklar arası mesafe azaldıkça, analitlerin bağlanması üzerine LSPR tepe kaymalarının azaldığı gözlendi. Öte yandan, AR azaldıkça, GNR'lerin LSPR yanıtı maviye kaydı. Bu tezde sunulan sonuçlar, çeşitli biyomedikal ve teşhis uygulamaları için LSPR tabanlı biyosensörlerin potansiyelini geliştirmeye yönelik gelecekteki araştırmalara katkıda bulunabilir.

To my dear sister Şule KILIÇ

TABLE OF CONTENTS

LIST OF FIGURES

Figure **Page**

LIST OF TABLES

Table

Page

ABBREVIATIONS

Symbol	Description
LSPR	Localized Surface Plasmon Resonance
CTAB	Cetyl Trimethyl Ammonium Bromide
SaM	Self-Assembled Monolayer
SEM	Scanning Electron Microscope
OEG	Oligoethylene Glycol
UV-Vis	Ultraviolet-visible
LPB	Longitudinal Plasmon Band
TPB	Transverse Plasmon Band
PEG	Polyethylene glycol
SPs	Surface plasmons
AuNRs	Gold nanorods
GNRs	Gold nanorods
GNP	Gold nanoparticule
PBS	Phosphate buffered saline
RI	Refractive index
Λmax	Maximum wavelength
RIU	Refractive index unit

CHAPTER 1

INTRODUCTION

Biosensors are devices that combine biology's high sensitivity and specificity with physicochemical transducers to deliver sophisticated bioanalytical measurements in simple, user-friendly formats. The primary purpose of such a device is to generate a discrete or continuous digital electronic signal proportional to a single or group of bioanalytes (Turner 2013). The foundational description of the "enzyme electrode" by Leyland C. Clark in 1962 was the first to define the basic notion of the biosensor. Clark described glucose oxidase, which was immobilized on the surface of an amperometric oxygen electrode and may be directly monitored through a semipermeable dialysis membrane. Clark's basic design was so effective that it is still utilized in numerous research and at least one commercial biosensor (Sassolas et al., 2012; Newman et al., 2006).

The optical characteristics of metal nanostructures are used by localized surface plasmon-based (LSPR) biosensors to provide label-free and sensitive detection (Unser et al., 2015; Manzano et al., 2016). Biosensors using plasmonic nanoparticles with receptors that precisely attach to target biomolecules have caught the attention of researchers due to their label-free real-time and highly sensitive readings. The LSPR can be seen as a result of the interaction between incident light and the collective oscillation of free electrons on nanoparticle surface. In addition to noble metal nanoparticle type (Ahmadivand et al. 2015; Kadkhodazadeh et al. 2017), material shape (Ameer et al., 2016), size (Langhammer et al., 2007), and dielectric environment (Wang et al., 2018; Larson et al., 2019) affect the LSPR phenomenon.

Gold nanoparticles (GNPs) are one of the most studied nanomaterials. Because of their well-established and diverse synthesis processes, biocompatibility, simplicity of surface functionalization, and distinctive optical features, they have enabled a wide range of diagnostic and therapeutic applications (Cao et al., 2014; Wang et al., 2017). Despite the fact that biomolecule attachment to the surface of GNP results in easily detectable changes in the LSPR peak, this property has been utilized to create biosensor devices.

Gold nanorods (GNRs) exhibit highly sensitive tlocalized surface plasmon resonance (LSPR) response and offer an enhanced signal as a result of their anisotropic morphology. The utilization of GNRs is highly significant due to their adjustable optical characteristics, convenient surface functionalization capabilities, and compatibility with biological systems (Cao et al., 2014).

The anisotropy of gold nanorods (GNRs) causes the optical absorption bands to break into two different LSPR peaks, which correspond to resonances along the short and long axes of the bar and are referred to as transverse and longitudinal bands, respectively. The transverse peak is frequently more susceptible to changes in local refractive index than the longitudinal band. Furthermore, unlike GNPs, the aspect ratio influences the maximum absorption value of this peak (Mishra et al., 2018).

The response of localized surface plasmon resonance (LSPR) of nanorods is influenced by various factors, including the dimensions and shape of the nanorod, the refractive index of the surrounding medium, and the dielectric constant. Furthermore, the LSPR properties can be influenced by the presence of ligands or biomolecules that are bound to the surface of the nanorod. The significance of these parameters in enhancing LSPR sensor design is pivotal for enhancing sensitivity, expediting response time, and devising optimized biosensors for the detection of analytes at low concentrations (Cao et al., 2014, Cao et al., 2012).

The aim of this study is to investigate the impact of the aspect ratio and the interparticle distance of GNRs on the localized surface plasmon resonance (LSPR) response of glass sensor chips decorated with GNRs. The effect of $AgNO_3$ concentration on the size of GNRs, the effect of the stabilizer molecule type and molecular weight on the distribution of GNRs on glass surfaces, and the effect of the interparticle distance between GNRs and their aspect ratio on the LSPR response of GNRs were investigated. The results obtained from these investigations are summarized in Chapter 4.

CHAPTER 2

LITERATURE REVIEW

2.1. Biosensors

Biosensors are devices that are used in a variety of disciplines, including environment, food, medicine, and agriculture. A biosensor is a device that detects biological or chemical processes by generating signals proportional to an analyte concentration in the medium. According to IUPAC guidelines 1999, a biosensor is an independently integrated receptor transducer device that can offer selected quantification or semi-quantitative analytical information via a biological recognition element (Thevenot et al., 1999). It is simply a device that combines a biological or biologically derived recognition element to identify a specific bio-analyte with a transducer to convert a biological signal into an electrical signal (Lowe et al., 2007; Perumal, Hashim 2014).

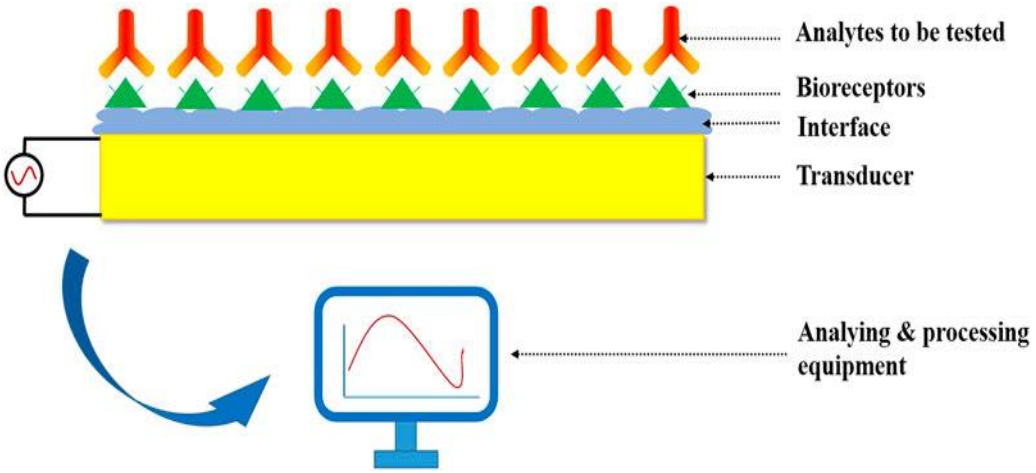

Figure 1. Illustration of a biosensor (Song et al., 2021).

The purpose of a biosensor is to provide rapid, real-time, accurate, and reliable information about the investigated analyte. Ideally, it should be a device capable of responding continuously, reversibly, and without disrupting the sample. Biosensors are

anticipated to play an important analytical role in medicine, agricultural production, food safety, national security, biotechnological processes, environmental monitoring, and manufacturing monitoring (Luong et al., 2008), (Figure 1). The main components of a biosensor are the bioreceptor, the transducer, and the signal processing system (David et al., 2010). A biological recognition element, also known as a "bioreceptor," is an immobilized biocomponent that can detect a particular target analyte. The majority of these biocomponents are antibodies, nucleic acids, enzymes, cells, etc. The transducer, in contrast, is a converter. The response between the analyte and the bioreceptor results in chemical changes, such as the formation of a new chemical, the emission of heat, the flow of electrons, and changes in pH or mass. The biochemical signal is converted into an electrical signal by the transducer. Eventually, the electrical signal is amplified and transmitted to a nanoelectronics and information processor. Produces a measurable signal, such as a digital display, transcript, or optical change.

2.2. Types of Biosensors

Biosensors can be divided into numerous categories. This is due to the fact that biosensors provide us a wide range of benefits and can be put to use in a wide variety of contexts. Optical, mechanical, and electrochemical signal transmission mechanisms, as well as different bioreceptor types, are all used to categorize biosensors. Biosensors are instruments where the bioreceptor-analyte molecular interaction plays a crucial role in triggering a reaction (Goode et al., 2015). Enzyme biosensors, tissue biosensors, immunosensors, DNA biosensors, thermal biosensors, and piezoelectric biosensors are just a few examples of the many types of biosensors available. Sensor selectivity and sensitivity can be optimized by careful design. Due to their low cost, great stability, and high specificity, biosensors are the preferred devices (Table 1).

Table 1. Classification of biosensors based on signal transduction and biorecognition (Source: Alhadrami, 2018).

Recognizing Biomolecule	**Example**	**Signal Transduction**	**Example**
Antibodies (Immunosensors)	• Monoclonal • Polyclonal	Electrochemical	• Amperometric • Conductimetric • Impedimetric • Potentiometric
Protein Receptor	• Metabotropic receptors • Ionotropic receptors	Optical	• Absorbance • Fluorescence • Phosphorescence • Bio/chemiluminescence • Reflectance • Raman scattering • Refractive index
Enzymes	• β-glucuronidase (encoded by gusA marker gene) • β-galactosidase (encoded by lacZ marker gene)	Mass sensitive	• Surface acoustic wave biosensor • Cantilever biosensors
Whole cell	• Microbial sensors • Mammalian cells tissue	Optical	• E. coli K12C600 • E. coli HB101 • E. coli DPD1718
Nucleic acids	• Hybridization • DNA-aptamers based biosensors	Optical (Fluorescence)	• Fluorescence-based aptasensor

2.2.1. Optical Biosensors

High sensitivity, dependability, and the possibility of a single-chip design are just a few of the benefits of optical biosensors. Optical biosensors are sensors that rely on the detection of ultraviolet (UV), visible, or near infrared (NIR) absorption, reflection, or fluorescence emissions. Surface Raman scattering (SER), localized surface plasmon resonance (LSPR), electroluminescence (EL), colorimetry, fluorescence (fluorescence), and chemiluminescence (CL), are all used in the development of optical biosensors (Wu et al. 2022), (Table 2).

Table 2. A brief description of the optical biosensing method of operating principles.

Biosensor technique	**Working principle**	**Measured signal**
Resonance-based optical sensors • SPR based sensors • LSPR based sensors	Surface plasmons occur when polarized light contacts a conductive surface. An analyte's binding to the metal surface's biorecognition element affects the dielectric's refractive index. This alters the propagation constant of surface plasmons, causing angular modulation or concentration-dependent wavelength modulation.	Change in refractive index
Fiber-based sensors • PCF based sensors • Interferometer and grating based biosensors • Resonator based biosensors	An optical fiber-based biosensor is a fiber bundle that serves as a platform for the biological recognition component and a conduit for excitation light and/or the output signal.	Optical power density
Colorimetric biosensors	For quantitative analysis, colorimetric biosensors can be used to identify a specific analyte based on color changes that are visible to the human eye (Zhao et al., 2020).	Measurement of color density

(cont. on next

Table 2. (cont.)

Fluorescence based biosensors	A fluorescence is a molecule that absorbs electrical energy and, when released, emanates light with a different wavelength. The concentration of the molecule affects the luminosity and decay rate of the re-emitted light.	Fluorescence intensity
Terahertz based biosensors	Hydrogen bonding and van der Waals forces cause low-frequency molecular vibrations in THz biological applications.	Frequency based measurement
Electrochemiluminescence, chemiluminescent biosensor	Determines the strength of the light that a chemical reaction produces.	Light intensity
SERS based sensors	Raman scattering happens when light excites a molecule inelastically. This creates a molecule-specific spectrum with peaks inversely proportional to concentration. Surface-Enhanced Raman Spectroscopy increases weak Raman scattering signals by using rough metal surfaces.	Intensity of peaks in Raman spectrum

The resonance-based optical sensors include two types of biosensors: surface plasmon resonance (SPR) and localized surface plasmon resonance (LSPR)-based biosensors. SPR is a technique used to examine changes in the refractive index on a metal surface. When light is exposed to a thin metal surface at a particular angle of incidence, it causes the conduction electrons to oscillate coherently and the formation of a surface plasmon wave (Wu et al., 2022).The incidence causing surface plasmon resonance depends on the refractive index of the surface, which makes SPR a powerful tool for biosensing applications. On the other hand, when surface plasmons are confined to nanoparticles that are smaller than the wavelength of light, the phenomenon is called LSPR. Upon binding of molecules to the noble metal nanoparticle surface, a shift in the

maximum absorption band occurs. The shift in the peak form the basis of biosensing via LSPR (Chen et al.,2020, Kaur et al., 2022).

Photonic crystal fibers (PCF), fiber bragg gratings (FBG), and interferometric sensors are fiber-based. In the PCF technique used to direct the light, it is aimed to direct the light refractive index with the air holes placed at equal intervals. Interferometric biosensors are nano-oprode optical sensors with large grids. Interferometric biosensors include measurements obtained by comparing the refractive index with bioconjugate interaction and the non-specific refractive index. Resonator-based biosensors are a type of sensor that creates optical micro-cavities and traps light in these spaces and creates optical signals depending on the light intensity (Campbell 2008).

Colorimetric biosensors are devices where the interaction of the target molecule with chemo-responsive dyes makes a noticeable difference. It is based on the principle of measuring absorbance and reflection by taking advantage of this color change, which is a result of the interaction.

For the purpose of measuring different enzymatic and small molecule activity, fluorescent biosensors have been developed. Fluorescent biosensors frequently use proteins with specific light-emitting characteristics, such as altered forms of green fluorescent protein (GFP) (Lai et al., 2017).

Terahertz (THz) waves are used in terahertz-based biosensors since they have low photon energy and don't ionize biological material. THz waves include electromagnetic waves that have a frequency between 0.1 and 10 THz. Relative to visible and close waves, THz waves have longer wavelengths, longer penetration depths, and less scattering (Vafapour et al., 2020). Electrochemiluminescence (ECL) emits photons using electrodes. Chemical reactions emit photons in chemiluminescence.

SERS can accurately identify single molecules. Molecular Raman signals near metallic nanostructures are amplified (Kahraman et al., 2017).

Each sensing method among the optical biosensor platforms in use has pros and cons and is still being developed.

2.3. Theory of LSPR

When an incident electromagnetic field is introduced to nanostructures with sizes smaller than or comparable to the wavelength of the incident mölight, the movement of oscillating electrons is trapped within the conducting nanoparticles, leading to the absorbance of light and the appearance of extinction bands. This optical phenomenon is known as Localized Surface Plasmon Resonance (LSPR). The phenomenon arises from the coupling between surface electrons in a conduction band and incident light. As a result of absorbing photon energy, the noble metal nanostructure shows different attenuation and near-field amplification characteristics.

When the LSPR is activated, the noble metal nanostructure's extinction spectrum will reach its maximum. The resonance wavelength in LSPR is affected by the difference in refractive index between the nanostructure and the surrounding medium.

Even though spherical gold nanoparticles have been initially used in LSPR-based biosensing applications, anisotropic particles, particularly gold nanorods (GNRs), are taking over their role. The two dimensions of GNRs result in two absorption bands, one due to transverse localized surface plasmon resonance (t-LSPR) and the other, much more favorable, due to longitudinal localized surface plasmon resonance (l-LSPR). Indeed, spherical gold nanoparticles have a unique LSPR band at 520 nm. The LSPR band is present at higher wavelengths, which correspond to either the first (650–950 nm) or second (1000–1350 nm) biological window. The position of the LSPR band can be adjusted by adjusting the AR of GNRs rather than their length. As a result, GNRs are now ideal candidates for a wide range of biomedical applications. GNRs have been shown to be adaptive and versatile actors, enabling transduction read-out in a range of settings. Their use in biosensing and other biomedical applications is increasing considerably.

2.4. Properties of Gold Nanorods

Gold nanoparticles, gold nanorods, gold spheres, etc. are widely used in optical sensor systems because of their high stability when exposed to light. Noble metal nanoparticles form structures with different widths, lengths, and shapes. The ability to control width, height, and shape properties with different synthesis methods attracts a lot of attention in areas such as biosensing, photothermal therapy, biosensors, and molecular imaging. Gold nanorods are rod-shaped nanoparticles. Gold nanorods attract

attention due to their optical and plasmonic properties. One of the main reasons for the use of GNRs is their higher reactivity compared to spherical particles. An increase in sensitivity to target molecules is observed with this feature. The luminescence and electrochemical properties differ depending on the size of the nanorods. For this reason, the fact that nanorods can be synthesized in a controlled manner provides great convenience (Chirea et al.,2009, Toderas et al., 2009). The unusual optical and electronic features of anisotropic plasmonic nanoparticles have attracted substantial attention in several studies. These features include strong absorbance in the near-infrared region, increased efficiency in light coupling, and a notable enhancement in the signal of surface-enhanced Raman spectroscopy. Gold nanorods have garnered significant interest due to their unique nanoplasmonic features and successful applications in biomedical contexts, including photothermal treatment, drug administration, imaging, and sensing. One of the primary characteristics of GNRS is the longitudinal-localized surface plasmon resonance (L-LSPR), arising from the coherent and collective oscillation of valence electrons along the longitudinal axis caused by light. Consequently, a distinct and highly concentrated absorption of light occurs across a broad range of wavelengths. This optical feature is heavily influenced by the aspect ratio of the rod, which may be tailored by a controlled synthesis process.

Many studies are being carried out to increase the efficiency of gold nanorods that can be used in applications in the fields of nanomedicine, biological sensors, and optical devices. In addition, changes in the shape of gold nanorods allow their physical and chemical properties to be manageable. The main difference between spherical and non-spherical gold nanoparticles is their ability to exhibit anisotropic optical and electronic responses determined by their topological properties. For this reason, gold nanorods attract a lot of attention and are the subject of studies in terms of their ability to exhibit anisotropic optical and electronic responses (Figure 2). (Chen et al., 2013).

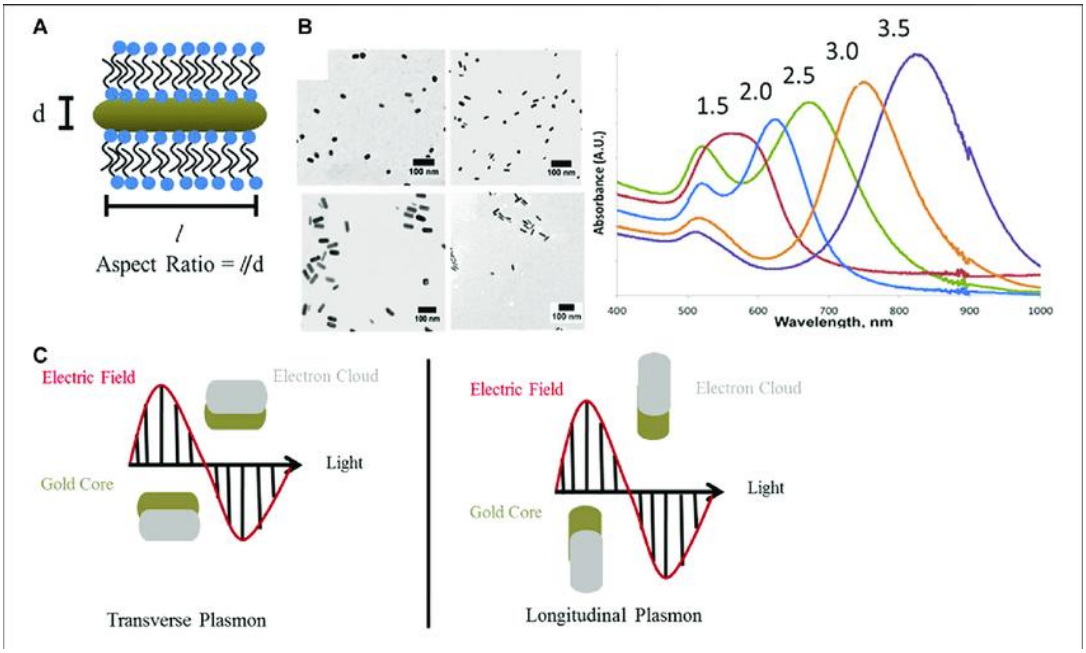

Figure 2. GNR optical features include transverse and longitudinal surface plasmon resonance bands. Aspect ratios which is the ratio of length to diameter affect longitudinal plasmon resonance band. (B) TEM images and UV, visible, and infrared extinction spectra of GNRs with ARs from 1.5 to 3.5; ARs are indicated above each absorbance spectrum. Scale bars are 100 nm. GNR transverse and longitudinal plasmon absorbances are shown in (C). Liao et al. (2021).

2.5. Synthesis of Gold Nanorods

Due to their good biocompatibility and adjustable stability, gold nanoparticles have been successfully used in many biomedical, medical and therapeutic fields. It is a great advantage that the shape and size of gold nanoparticles can be adjusted in a controlled manner. Since this feature adds designability to gold nanoparticles, it enables them to design and utilize their optical, electrical, catalytic, and magnetic properties as desired (Jiang et al., 2013).

There are different methods for the synthesis of gold nanorods. The seed-mediated growth method has been the most popular method among the most widely used approaches because it is inexpensive and provides high efficiency synthesis.

The seed-mediated growth method consists of two steps. At the first step, the nanoparticle seeds are produced, and at the second step, the nanoparticles with desired shape are obtained. The synthesis of non-spherical nanoparticles is carried out using cetyl trimethyl ammonium bromide (CTAB), the most popular surfactant in the seed solution. Micelles formed by surfactants play a role in shaping nanoparticles and act as a matrix.

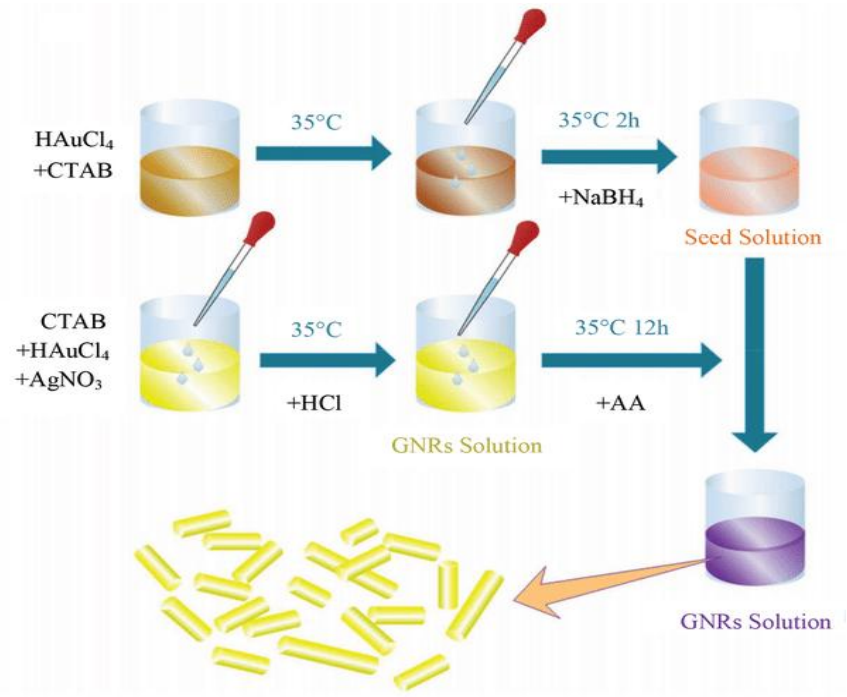

Figure 3. Schematic of a seed-mediated growth for GNRs (Source: Fu et al. 2021).

Murphy and his colleagues worked a lot on this method to generate GNRs (Figure 3). The first step is to make a seed solution by reducing hydrogen tetrachloroaurate with sodium borohydride in the presence of sodium citrate. This is the process of preparing the seeds and stabilizing them. Then, during the second stage of seed growth, the seeds are put in a solution with hydrogen tetrachloroaurate, CTAB, and ascorbic acid and left there to grow. By changing the conditions of the synthesis, it is possible to make gold nanorods with different lengths and widths. MA El-Sayed and his colleagues were the first to suggest using CTAB as an AuNR stabilizer and adding some silver nitrate to the reaction mixture to control synthesis (9). KJ Murphy and his colleagues have reported how the ionic strength of the growth solution affects the parameters of the nanoparticles that are made. Many studies have been performed to

improve the seed-mediated growth method, which is still one of the most used methods. Gold nanoparticles can vary in size, form, and where they are found depending on a number of factors. Some of these factors are the amount of CTAB and other reagents, the reaction time, the pH, or the temperature. By adjusting these factors, it is possible to make gold nanoparticles with different widths, lengths, and shapes.

CHAPTER 3

MATERIALS AND METHODS

3.1. Materials

Chemicals: Ascorbic acid, hydrogen tetrachloroaurate (III) hydrate ($HAuCl_4$), hydrogen peroxide (H_2O_2), sulfuric acid (H_2SO_4), sodium borohydride ($NaBH_4$), silver nitrate ($AgNO_3$), and hydrogen peroxide (H_2O) were purchased from Sigma Aldrich which also provided potassium carbonate and methoxypolyethylene glycol thiol ($mPEGSH_{5000}$ and $mPEGSH_{2000}$). Hexadecyl trimethyl ammoniumbromide (CTAB) was purchased from Alfa Aesar. Alkanethiols, 11-mercapto-undecanol and 23-9 mercapto nonyl-3,6,9,12,15,18,21-heptaoxatricosanoic acid were purchased from Sigma Aldrich and Santa Cruz Biotechnology. Sigma Aldrich supplied ethanol and aminopropyltriethoxysilane (APTES). A Millipore Milli-Q Plus water purification system with a 0.22 m filter was used to obtain distilled water. The microscope slides were purchased from ISOLAB.

Instruments: The FEI Quanta 250 FEG in the Materials Research Center (MAM) at IZTECH was utilized for scanning electron microscopy (SEM) analyses. The Perkin Elmer UATR Two instrument in the Biotechnology and Bioengineering Research and Application Center (BIOMER) at IZTECH was utilized for FTIR spectroscopy. For oxygen plasma treatment, a Diener Zepto low-pressure plasma machine was employed. Hettich Mikro centrifuge equipment was employed for centrifugation of gold nanorods. An Ocean Optics USB2000+ spectrometer connected to an Olympus light microscope was utilized as a localized surface plasmon resonance spectrometer.

3.2. Methods

3.2.1. Synthesis and PEG'ylation of Goldnanorods

Gold nanorods (GNRs) were synthesized by the seed-growth method, which is one of the most well-known synthesis methods (Nikoobakht and El-Sayed, 2003). In

this two-stage synthesis method, the seed solution was first prepared using $HAuCl_4$ (0.001 M, 2.5 ml), CTAB (0.2 M, 5 ml), and $NaBH_4$ (0.01 M, 600 µl).

Since CTAB is a substance that crystallizes at room temperature and hardly dissolves, it was first left to melt in a hot water bath for 3 hours. The seed solution composed of $HAuCl_4$, CTAB and $NaBH_4$ was left to stir on a magnetic stirrer for 2 hours.

At the next step, the gold nanoparticles formed in the seed solution was transformed into gold nanorods by mixing $HAuCl_4$ (60 mL, 0.01 M) dissolved in distilled water, CTAB (60 mL, 0.2 M), $AgNO_3$ (300 µL, 0.032 M), ascorbic acid (840 µL, 0.079 M) and 180 µl of seed solution. The final solution was mixed overnight on a magnetic stirrer and the color change was observed. To vary the aspect ratio (AR) of GNRs, the amount of Ag+ ions was changed in the growth solution (Jana et al., 2001) The volume of 0.032 M of AgNO3 was varied in the range between 20 and 350 µl, to demonstrate the influence of $AgNO_3$ on AuNR aspect ratio. 55 µl of 0.1 M ascorbic acid was also added to the solution.

The GNRs synthesized with the above-given procedure contained CTAB as the surface stabilizer. In order to investigate the effect of the surface coating molecules' type and molecular size on the distribution of GNRs on the silanized glass surface, CTAB on the surface of GNRs was exchanged with methoxypolyethylene glycol thiol having two different molecular weights ($mPEG_{2000}$-SH and $mPEG_{5000}$-SH). CTAB molecules on the surface of GNRs were first removed by centrifugation at 12000 rpm. mPEG-SH solution (2M, in 120 µl deionized water), GNR solution (0.01M, 6ml) and potassium carbonate solution (2M, 120 µl deionized water) to prevent the rods from collapsing, was mixed. It was left in the magnetic stirrer overnight. PEGylated GNR was then centrifuged (at 12000 rpm) to remove excess PEGs. After centrifugation, the supertanant was removed and deionized water (1, 2 or 3 ml) was added to the pellets. Then, the glasses that will form the sensor chip surface were placed in this solution.

3.2.2. Functionalization of Glass Surfaces with GNRs

The glass microscope slides were used to construct the sensor chips. For the preparation and cleaning of the glass surface, the microscope slide was divided into 6 pieces, each approximately 8x15 mm, with a diamond-tipped glass pen. Broken glasses

were placed in a Piranha solution (CAUTION: Piranha solutions are VERY DANGEROUS! In addition to being a corrosive liquid and strong oxidizer, it may cause dangerous foaming, explosion, burning of organic compounds. enormous quantities of heat and gas) consisting of 5 ml of hydrogen peroxide and 15 ml of sulfuric acid at a ratio of 1:3 in order to clean the organic residues and dust and to activate the -OH groups. After waiting for 30 minutes in the piranha solution, the removed glasses were repeatedly washed with distilled water and dried with nitrogen gas. The cleaned glasses were immersed into the aminopropyltriethoxysilane (APTES) solution (99% purity ethanol) and kept in the solution for 3 hours. After 3 hours, the glasses were removed from the solution and washed first with ethanol and then with deionized water and dried with nitrogen gas. At the next step, glasses coated with APTES were immersed in the GNR solution (1 mL) and left for 1 day to modify the the glasses with GNRs. To investigate the effect of aspect ratio (AR) on LSPR response, GNRs (PEGylated with mPEG-SH5000) having an AR of 4, 6 and 8 were utilized. To vary the interparticle distance of PEGylated GNRs placed on the glass surfaces, GNR (PEGylated with mPEG-SH5000, AR= 4, 6 and 8) solutions prepared at varying dilutions as described in Section 3.2.1 were utilized. The next day, the glasses were washed with deionized water and dried with nitrogen gas. The color of the glasses was observed to adopt the color of the GNR solution. Finally, oxygen plasma treatment was performed to remove PEG from the surface of the GNRs. During this process, the glasses were kept for 30 seconds in a 100 W oxygen plasma device under 200 mTorr pressure.

3.2.3. LSPR Response Measurement of GNR Modified Glass Surfaces

The LSPR response of glass surfaces modified with GNRs having varying aspect ratios and interparticle distances was measured using self-assembling alkanethiol molecules containing –OH and –COOH functional groups. 11-mercapto-undecanol and 23-9 mercapto nonyl-3,6,9,12,15,18,21-heptaoxatricosanoic acid were utilized. First, 11-mercapto-undecanol and 23-9 mercapto nonyl-3,6,9,12,15,18,21-heptaoxatricosanoic acid were dissolved in ethanol. The final solution contained 16-Mercaptohexadecanoic of 0.5 mM and 11-Mercapto-1-undecanol of 4.5 mM (the mole ratio of 11-mercapto-undecanol and 23-9 mercapto nonyl-3,6,9,12,15,18,21-

heptaoxatricosanoic acid was 9:1). The GNR modified glass chips were then immersed in the solution overnight at room temperature. The solution was kept in dark. After the incubation period, the glasses were washed with deionized water and then LSPR measurements were performed to observe the absorption of molecules. The LSPR measurements were taken using An Ocean Optics USB2000+ spectrometer between 800 and 1200 wavelengths. The wavelength at the maximum absorption (λ_{max}) was recorded as LSPR signal. Each experiment was repeated independently at least 3 times. The LSPR signals were reported as the mean ± standard error of 10 different measurements of the glass surfaces obtained from 3 independent experiments.

3.2.4. Characterization of GNRs and Glass Surfaces

3.2.4.1. Scanning Electron Microscopy (SEM)

The GNRs sizes and distribution on glass surfaces were examined using SEM. SEM images were captured using an FEI Quanta 250 FEG microscope at a voltage of 2 kV.

3.2.4.2. Fourier Transform Infrared (FTIR) Spectroscopy

The modification of GNRs with PEG molecules were confirmed using FTIR spectroscopy. The Perkin-Elmer Universal Attenuated Total Reflectance (UATR) technique is a widely used method in analytical chemistry for the characterization of solid samples. Employed to characterize the molecules present on the surface both before and after modifications. The measurements were conducted both prior to and subsequent to the application of PEG and oxygen plasma treatment, as well as on surfaces that had undergone OEG- Alkanethiol.

3.2.4.3. Vis-NIR Spectroscopy

Vis-NIR spectroscopy was used to determine shift values to measure changes on the biosensor surface. Vis-NIR spectroscopy was used to determine shift values to measure changes in the biosensor surface. Ocean Optics USB2000+ spectrometer measuring between 800 and 1200 wavelengths was used.

CHAPTER 4

RESULTS AND DISCUSSION

4.1. Synthesis of GNRs with Varying Aspect Ratios

Adjusting $AgNO_3$ concentrations is the most common way to change the aspect ratio (AR) of GNRs. While the role of Ag^+ ions in the anisotropic growth of GNRs is still unknown, it is commonly (Lohse et al., 2013; Scarabelli et al., 2015; Jancson et al. 2014; Tong et al., 2017; Zhang et al., 2016) believed that it is caused by the underpotential deposition mechanism or the joint reduction of gold and silver ions (so-called codeposition). Another possibility is that the anisotropic growth is due to the selective adsorption of the CTA^+ -Br^- -Ag^+ complex. Furthermore, silver ions may promote the transformation of spherical CTAB micelles into cylindrical ones (Lohse et al., 2013). It is also possible for several mechanisms to work together (Salavaton et al., 2018).

In this study, the ARs of the GNRs was varied by changing the $AgNO_3$ concentration of the growth solution (Manohar et al., 2016). Figure 4 shows the GNR solutions obtained with varying $AgNO_3$ concentrations (0,4μM, 0,5 μM, 0,6 μM, 0,7 μM AgNO3 in the growth solution). The size of the GNRs, especially the AR, effects the absorbance spectrum of the GNR solution. The size of GNRs synthesized by the seed growth method is controlled by the Ag ions adsorbed on the surface of the gold seeds and their growth as a result of redox reactions. This growth process takes place at different rates according to the size of the gold seeds and directly affects the size of the GNRs. As the size of the GNRs increases, the wavelength of the surface plasmon resonance (SPR) peak also increases. This affects the colors that the solution absorbs in the visible light spectrum. Generally, longer GNRs will have more red-shifted SPR peaks, while shorter GNRs may have more blue or green colored SPR peaks. Thus, changes in the size of the GNRs cause changes in the visible color spectrum of the solution. Figure 4 clearly shows the changing color of GNRs solution prepared by

changing the $AgNO_3$ concentration revealing the successful synthesis of GNRs having different ARs.

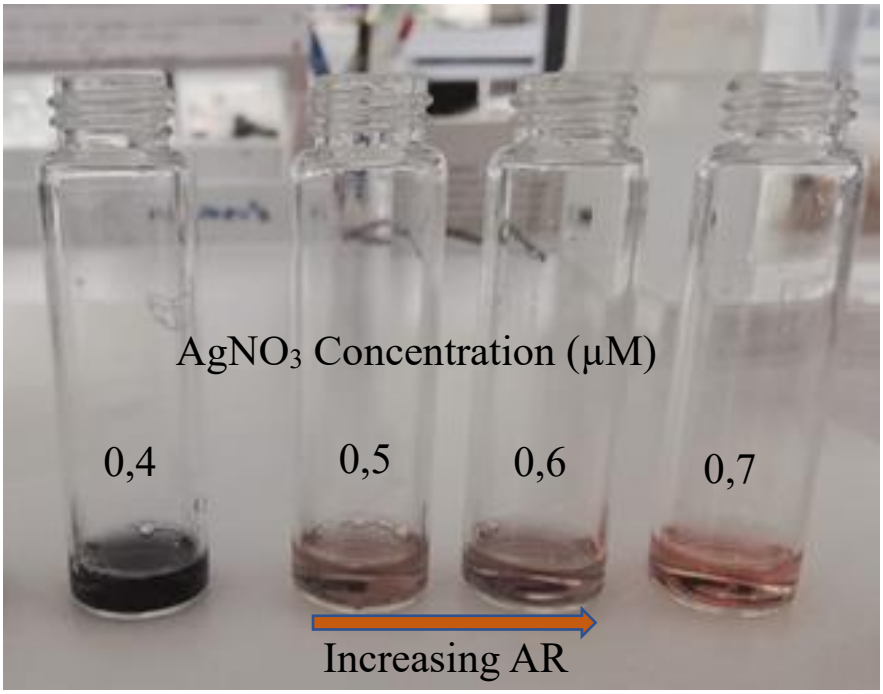

Figure 4. GNR solutions obtained by varying AgNO3 concentration in the growth solution. The color change indicates clearly the change in the GNRs' aspect ratio.

Figure 5 shows the LSPR absorption spectra of GNRs synthesized using different amounts of $AgNO_3$. The absorption spectra of GNR are well known to have two bands: the transverse plasmon band (λ_T) at 520 nm and the longitudinal plasmon band (λ_L) at a longer wavelength in the visible-NIR range. Because λ_L is primarily determined by the AR of GNRs. Figure 5 shows that λ_L is redshifted from 664 nm to 800 nm with increasing Ag concentration from 0,4 μM to 0,7 μM. The red-shift in λ_L with the increase in AgNO3 concentration directly confirms the increase in the AR of GNRs formed. These experimental results clearly demonstrate that the Ag content of the growth solution is critical for precise control of the AR of GNRs. It is worth noting that we were able to obtain reproducible GNRs under the same conditions from each synthesis series with a small deviation in λ_L (10-15 nm).

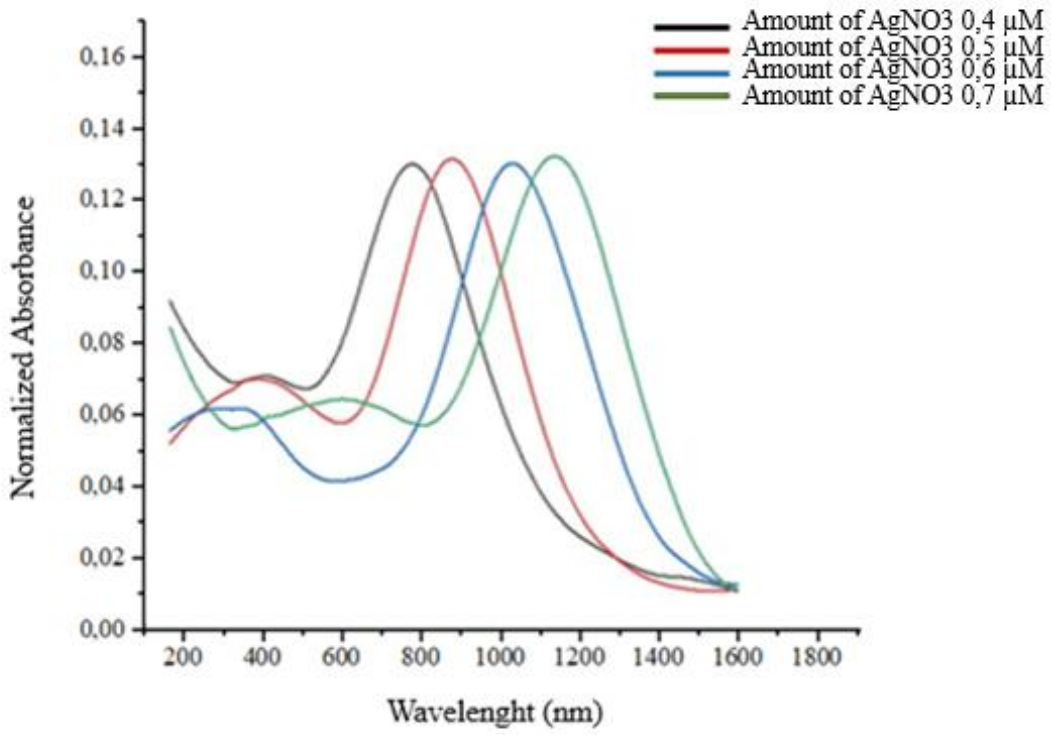

Figure 5. The LSPR spectra of the GNRs synthesized with varying $AgNO_3$ concentrations in the growth solution: the λ_L black, red, blue, and green is 650 nm, 820 nm, 1000 nm, and 1200 nm, respectively.

GNRs AR is clearly related to the wavelength of the longitudinal plasmon band (λ_L or λ_{max}). Equation 1 is the equation describing the relationship between the λ_{max} and the AR (R) (Cao, 2014). λmax and R in this equation refer to longitudinal plasmon peak and aspect ratio, respectively (Figure 5). This equation was used to calculate the AR of the GNRs synthesized in this study.

$$\lambda max = 95R + 420 \text{ (Equation 1)}$$

Accordingly, we obtained GNRs with ARs of 2.4, 4.2, 6.1, and 8.2 as tabulated in Table 3.

Table 3. The aspect ratio (AR) of GNRs synthesized using silver nitrate at varying concentrations.

$AgNO_3$ Concentration Used in Growth Solution (µM)	**Longitudinal Plasmon Peak (λmax)(nm)**	**Aspect Ratio (AR) Calculated via Equation 1**
0,4	650	2,4±0,5
0,5	820	4,2±1,0
0,6	1000	6,1±0,4
0,7	1200	8,2±0,5

Figure 6 shows the representative scanning electron micrographs of GNRs having varying ARs. The micrographs clearly showed the change in the AR of GNRs. The mean length and diameter of GNRs measured using the micrographs are given in Table 4. At least three different representative GNR SEM images of each sample were utilized to calculate the mean length, mean diameter and the standard error. On each micrograph, at least 100GNRs were measured.

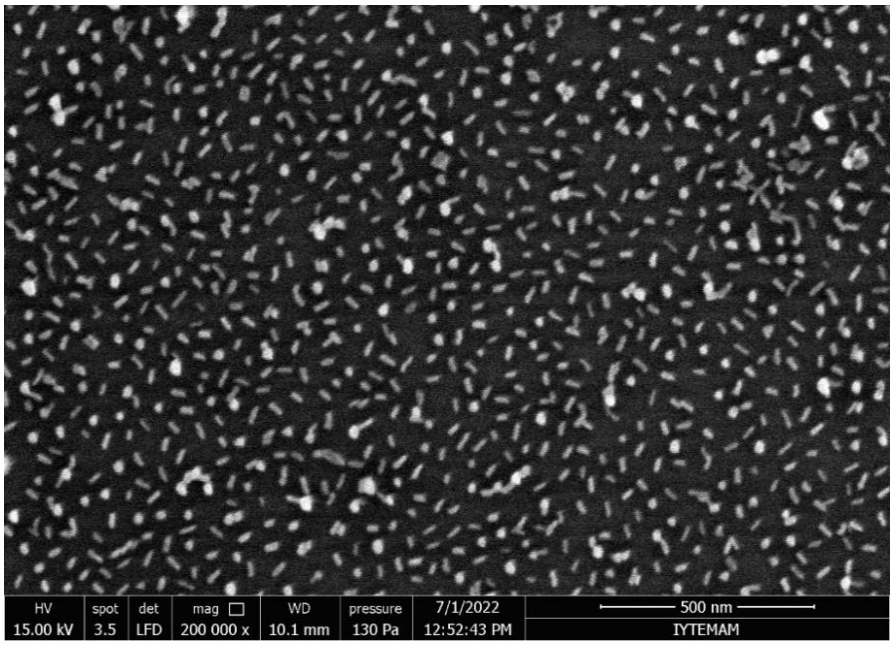

(cont. on next

Figure 6. (cont.)

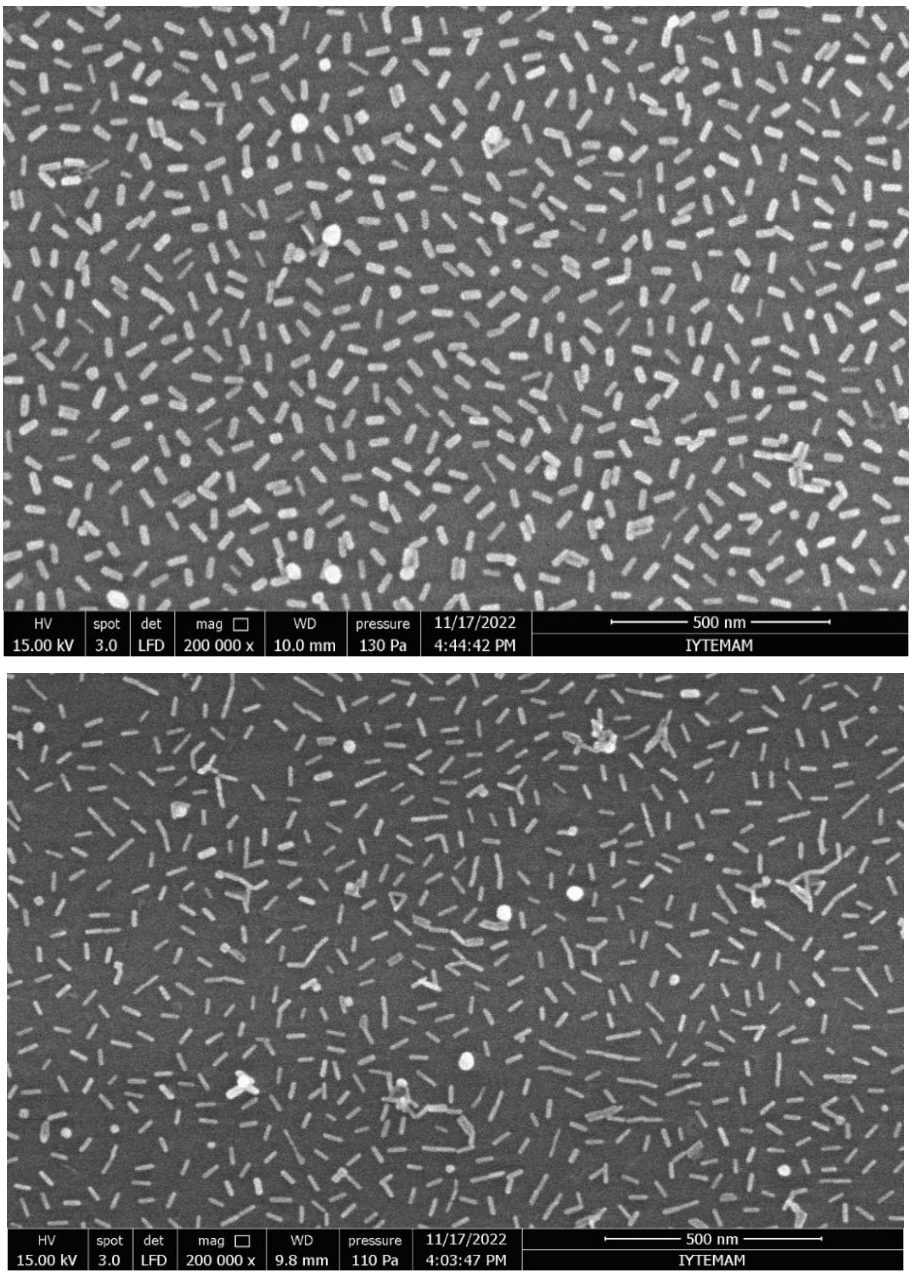

Figure 6. Scanning electron micrographs of GNRs with varying ARs.

Table 4. Dimensions of GNRs utilized for functionalization of glass surfaces to investigate the effect of AR on the LSPR response.

Aspect Ratio	Length and Width(nm) (determined from SEM images)*
4	**36(±6)** **16(±2)**
6	**45(±5)** **15(±4)**
8	**72(±8)** **13(±4)**

* N= Mean of at least 100 GNRs on at least three different SEM images

4.2. Preparation of PEG-coated GNRs

GNRs were synthesized in the presence of cetyltrimethylammonium bromide (CTAB) as a stabilizer. CTAB is a small, cationic and amphiphilic molecule having a molecular weight of 364.45 g/mol (Figure 7). To investigate whether using surface stabilizers with different molecular sizes affect the GNRs' distribution on silanized glass surfaces and hence control the interparticle distance, CTAB on GNRs was exchanged with mPEG-SH2000 and mPEG-SH5000 (Figure 7).

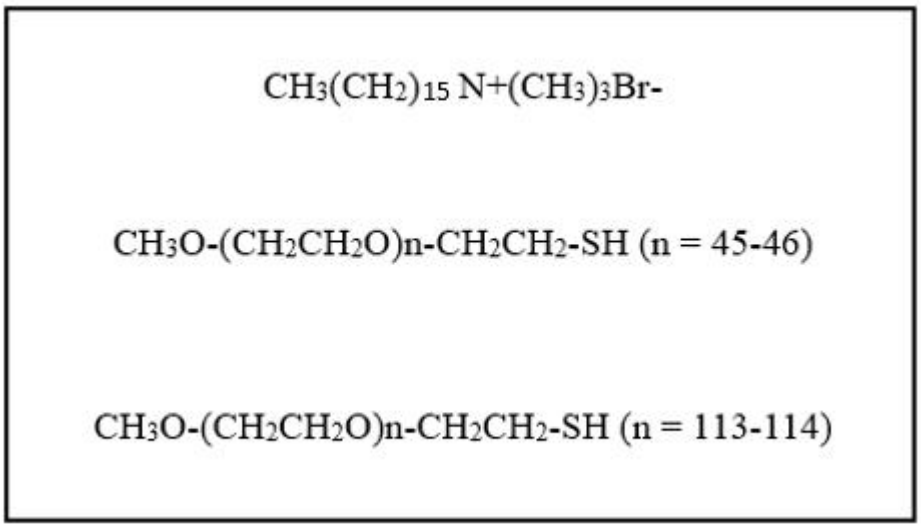

Figure 7. Chemical structure of CTAB (top), mPEG-SH2000 (middle) and mPEG-SH5000 (bottom).

CTAB is an effective substance that ensures the stability of gold nanoparticles. However, it forms a cationic layer on the GNR surface which maintains colloidal stability of GNRs through electrostatic repulsion. Therefore, the removal of CTAB destabilizes the GNRs, causing their aggregation in aqueous solution. Thiol-terminated PEG (polyethylene glycol) was used to replace CTAB. PEG is a highly hydrophilic neutral polymer which is frequently used to replace CTAB and maintain colloidal stability of GNRs in aqueous, especially physiological, solutions. CTAB replacement was performed using mPEG-SH through the formation of gold-thiol bonds. CTAB was removed using two-step centrifugation, and then GNRs were modified with mPEG-SH having two different molecular weights (2000 and 5000 g/mol). The LSPR (Localized Surface Plasmon Resonance) spectra of the GNRs before and after PEGylation are shown in Figure 8. From the LSPR spectra of GNRs before and after PEG'ylation with mPEG-SH5000, it can be seen that that the LSPR peak wavelength experiences a noticeable redshift, indicating successful PEGylation when using mPEG-SH5000. On the other hand, when mPEG-SH2000 was used, the LSPR band broadened and the peak maximum slightly blue-shifted, suggesting possible aggregation behavior of GNRs. This might be due to the insufficiency of the short PEG chains to stabilize and suspend GNRs in aqueous solution. The modification of GNRs with PEG molecules was confirmed using Fourier Transform Infrared (FTIR) spectroscopy (Figure 9). The FTIR

spectroscopy analysis involved comparing the FTIR spectra of the GNRs before and after the PEGylation process. Significant changes were observed in the FTIR spectra after PEGylation, indicating the successful attachment of PEG molecules to the GNR surfaces. These changes included the appearance of new characteristic peaks or shifts in existing peaks, which are indicative of the presence and bonding of the PEG molecules.

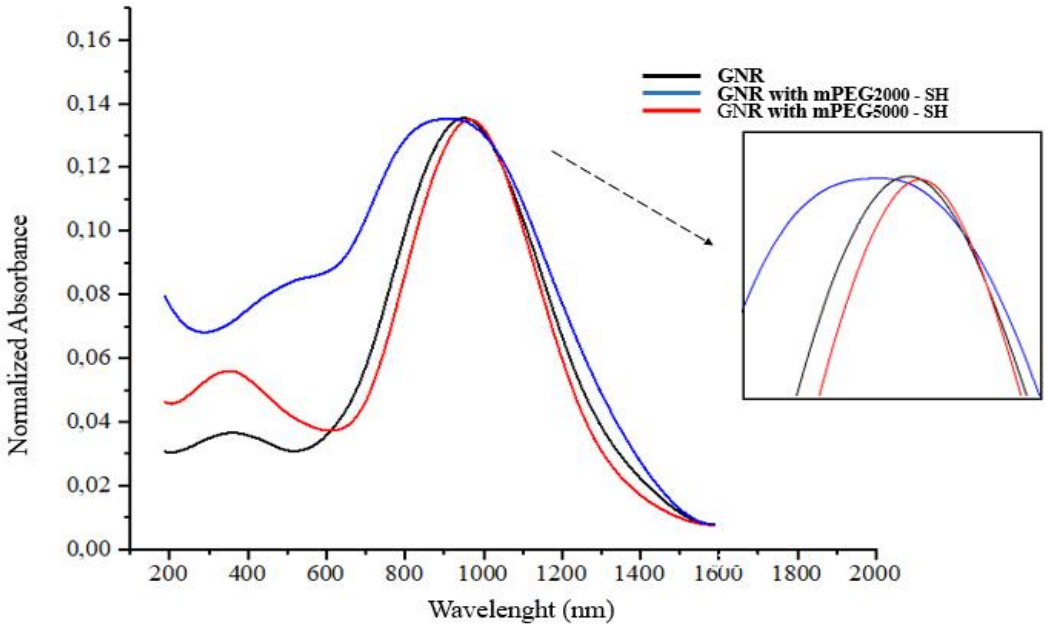

Figure 8. LSPR spectra before and after PEGylation of GNR with mPEG2000 -SH, mPEG5000 -SH.

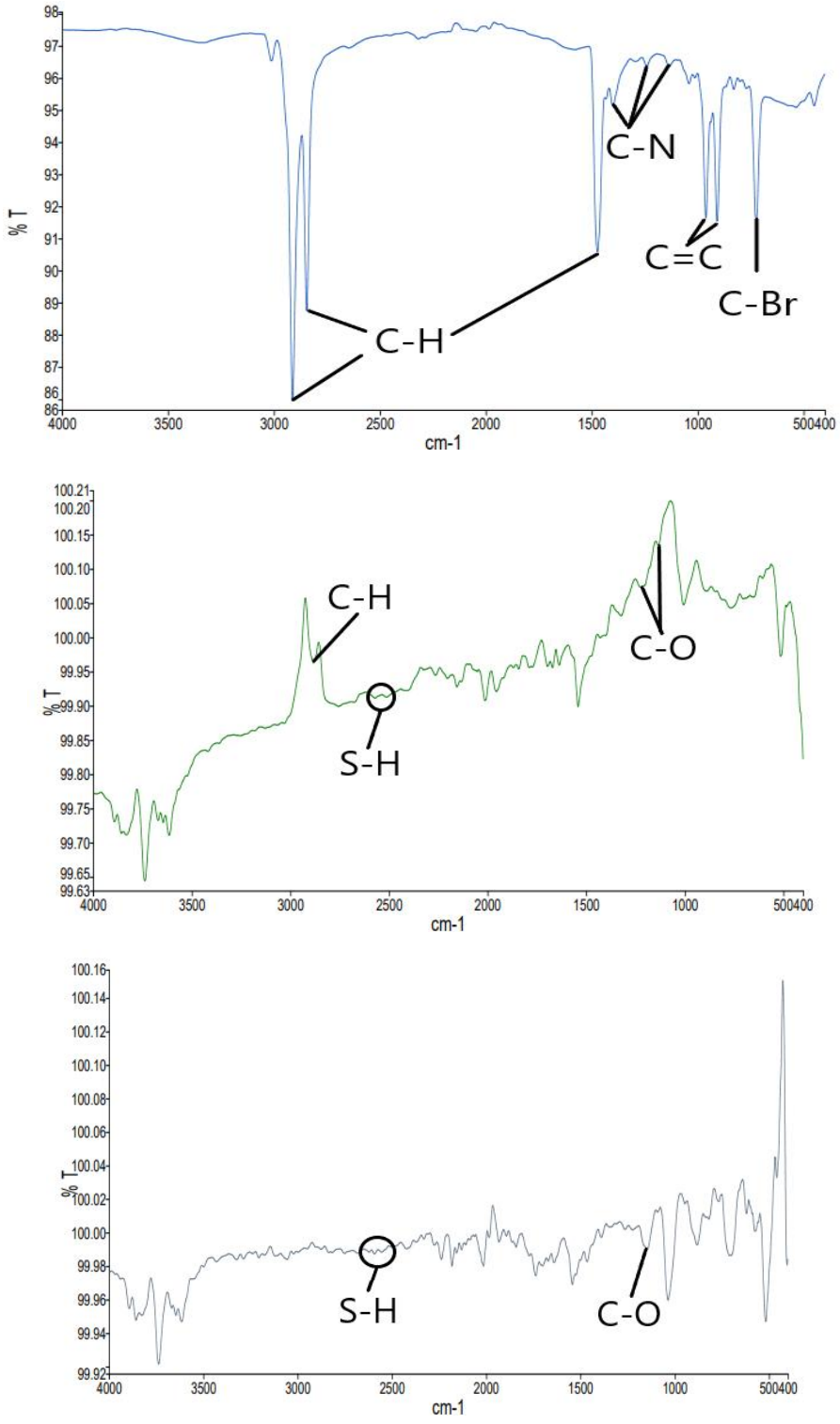

Figure 9. FTIR spectrum of CTAB, PEG 2K and PEG 5K illustrating characteristic absorption bands.

Before surfactant exchange, CTAB molecules were clearly observed on FTIR spectrum. PEG-GNRs have infrared (IR) absorbance peaks, which are assigned as

follows: 2,850–3,000 cm−1(–CH2 stretching), 1,380 cm−1(C–H bending; –CH2 and –CH3), 1,100 cm−1(C–O–C stretching), and 700–900 cm−1(N–H wagging) (Seol et. Al., 2012), (Figure 9). These peaks match the spectrum of PEG, showing PEG adsorption onto GNRs. After PEGylation with both PEG2000 and PEG5000, the bands that appear indicate the presence of PEG on the surface of GNRs. There were no peaks characteristic of CTAB on GNRs in the FTIR spectra. In conclusion, CTAB was completely removed from GNRs and GNRs were efficiently coated with PEGs.

4.3. Coating of Silanized Glass Surfaces with GNRs

Microscopic glass slides were utilized to prepare sensor chips. Initially, a piranha solution was used to purify slides by eradicating organic residues and impurities. Piranha solution which comprises a blend of sulfuric acid and hydrogen peroxide has also the role of facilitating the hydroxylation of the surface. The process of hydroxylation holds significant importance in facilitating subsequent surface modification with silane molecules. The chemical reaction between silane molecules and surface hydroxyl groups results in the formation of Si-O-Si bonds. After silanization of the glass surfaces using APTES following protocols reported in the literature (Söylemez 2020, Taykoz 2020), the silanized surfaces were coated with GNRs to investigate the effects of GNRs' interparticle distance and AR on the LSPR response of GNRs coated glass chips.

4.3.1 Controlling Interparticle Distance of GNRs on Glass Surfaces

To prepare GNRs coated glass surfaces with controlled interparticle distance, silanized glass surfaces were first treated with GNRs having CTAB, mPEG2000 or mPEG5000 as a surface stabilizer molecule. The glasses were immersed in a solution of GNRs for a duration of 24 hours. After incubation period of time, the surfaces were washed with deionized water several times and dried using nitrogen gas for SEM characterization. SEM micrographs of the surfaces after treatment with CTAB-, mPEG-SH2000 or mPEG-SH5000-stabilized GNRs are shown in Figure 10.

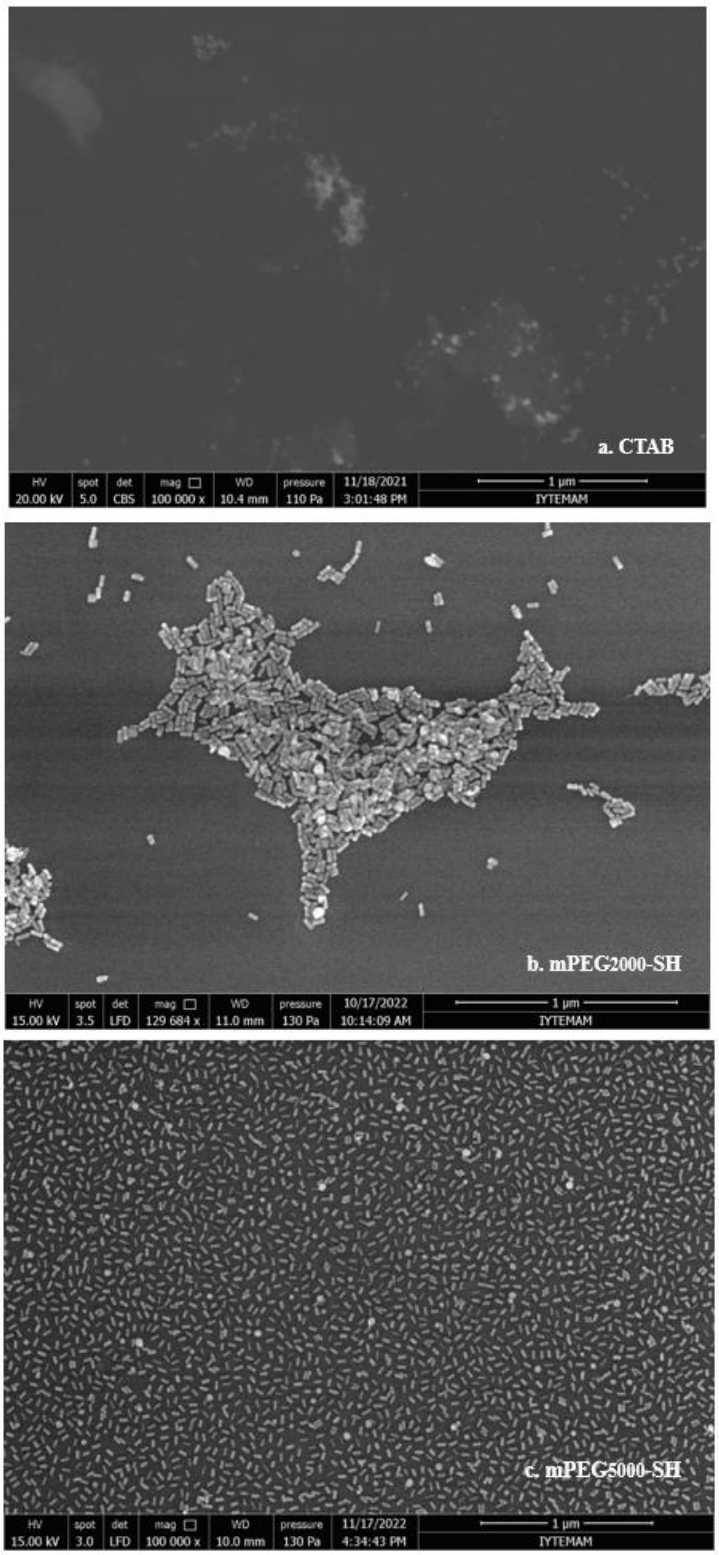

Figure 10. SEM images of the silanized glass surfaces after treatment with GNRs stabilized with (a) CTAB, (b) mPEG2000-SH and (b) mPEG5000-SH. Scale bar: 1 µm.

CTAB-stabilized GNRs appeared not to bind to the silanized glass surfaces, possibly due to the repulsive interaction between the positively charged CTAB layer and the positively charged silanized surface. When using GNRs with mPEG2000, gold clusters were observed on the surface via SEM. On the other hand, homogeneous distribution of nanorods on the surface was observed on SEM images when GNRs with mPEG5000 were used (Figure 10). In some studies, high dispersion properties of gold nanoparticles were observed when 2K PEG was used. This shows that PEG adsorbs on the surface of the nanoparticles and keeps the nanparticles away from each other by forming a sufficiently long distance between the nanoparticles and prevents aggregation. However, in our study, PEG2K did not stabilize the GNRs in aqeous solution well possible due to the bigger size of nanorods when compared with the ones reported in the literature (Burrows et al., 2016). On the other hand it was observed that PEG with 2K and 5K molecular weights had a different effect than expected on GNRs aggregation on the glass surface. The nanorods were well dispersed as the PEG chain length increased from 2K to 5 K. Such behavior is most likely caused by the formation of a sufficiently long enough PEG chain layer on the gold surface (Bogliotti et al., 2011), resulting in better particle dispersion based on increasing steric repulsive force as the PEG chain length increases(Drobek et al., 2005).There could be various factors contributing to the observed phenomenon, including the adsorption behavior of PEG molecules on the nanoparticle surface, hydrophobic interactions, hydrogen bonding ans steric hindrances of PEG molecules. It's probable that 2K PEG interact strongly with nanorods, but exerts less steric hindrance and is less powerful to prevent hydrophobic interactions between GNRs, which in overall will encourage aggregation.

The uneven distribution of gold nanorods on the surface may cause loss of optical properties. An example is the change or loss of surface plasmon resonance (SPR) property, as observed in the case of the surfaces treated with GNRs having mPEG2000-SH (Figure 11).

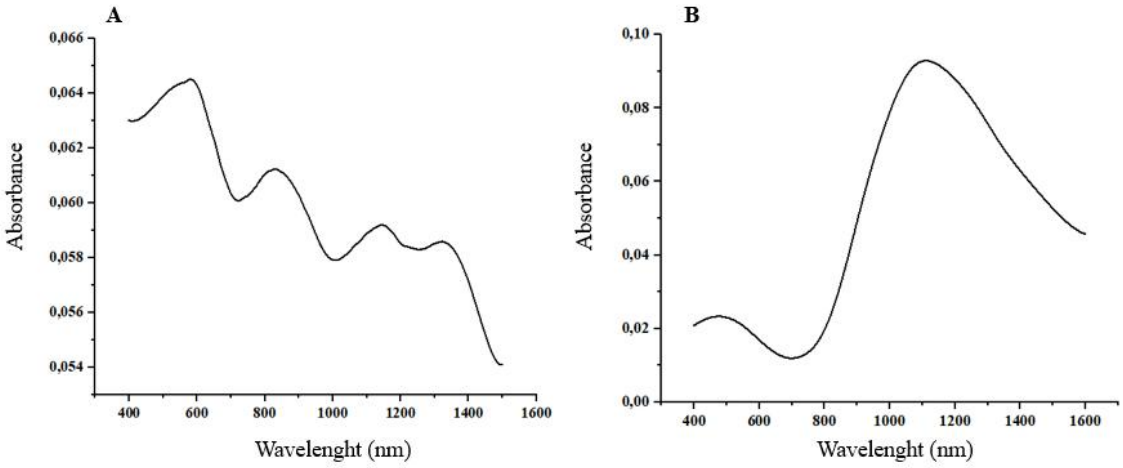

Figure 11. LSPR spectra of GNR coated glass surfaces: A) GNRs with PEG2000; B) GNRs with PEG5000.

LSPR is a spectroscopic technique that is commonly employed for the purpose of characterizing the optical properties and interactions of gold nanoparticles. The variance observed in the LSPR spectrum presented in Figure 11. can be attributed to the fluctuations in the surface distribution and aggregation states of the GNRs. When a uniform distribution of GNRs is present, as in the case observed with the surfaces trated with mPEG5000-SH coated GNRs (Figure 10 and Figure 11), the LSPR spectrum exhibits resonance at a specific wavelength. The correlation between the resonance wavelength and the sizes and shapes of the GNRs is evident. A specific distribution of GNRs induces a conducive setting for the activation and interplay of surface plasmons within the electromagnetic field. In instances where there is an aggregation or non-uniform dispersion of GNRs, alterations to the LSPR spectrum may occur. Aggregation refers to the phenomenon where GNRs coalesce to form clusters or assemblies. The act of grouping induces alterations in plasmonic interactions, leading to fluctuations in the spectrum of LSPR. The presence of an aggregation or non-uniform distribution of GNRs has the potential to alter or expand the resonance wavelength, thereby impacting plasmonic interactions. As a consequence, alterations in the LSPR wavelength occur. The interaction of GNRs with their surrounding environment and their electrical properties are altered in the aggregation state, leading to changes in the observed LSPR spectrum. To sum up, the systematic dispersion and consolidation of GNRs exhibit significant impacts on the LSPR spectrum. Hence, it can be inferred that the surface

distribution, aggregation state, and regularity of GNRs play a crucial role in determining the LSPR spectrum. When nanorods are close to each other, electromagnetic interactions get stronger, which changes the LSPR range. When nanorods get together, the plasmonic coupling effect between them gets stronger, and group plasmon resonance happens. Because of this, the LSPR spectrum is made up of a bigger range of wavelengths. However, there are certain drawbacks associated with the aggregation of nanorods. Firstly, when nanorods come into close proximity and form aggregates, their sensitivity and specificity can be compromised. The close contact between nanorods can lead to surface areas being partially or completely inaccessible, resulting in reduced interaction capabilities with proteins or other analytes. Additionally, aggregates consisting of nanorods with different surface features can alter specific binding interactions, making it more challenging for analytes to be effectively recognized and detected.

In addition, the presence of a broad range of LSPRs resulting from nanorod aggregation introduces challenges in spectrum analysis and interpretation. The composite spectrum may exhibit multiple overlapping plasmon resonances, which complicates the accurate determination and understanding of individual resonance contributions. Furthermore, nanorod clustering hinders their manipulation and controlled arrangement. Achieving consistent spatial positioning becomes difficult, impeding the reproducibility of measurements and limiting the ability to obtain consistent results across multiple analyses.

In conclusion, when CTAB or mPEG2000-SH was used as a stabilizer on GNRs, it was observed that the GNRs cannot be homogenously placed on the silanized glass surfaces used. On the other hand, mPEG5000-SH stabilized GNRs were homogenously distributed on the silanized glass surfaces, as evidenced by SEM images. Based on this result, GNRs having mPEG5000-SH were utilized in the rest of the study to functionalize the silanized glass surfaces.

At the next step, it was attempted to prepare GNRs coated glass surfaces with controlled interparticle distance by varying the GNRs solution concentration. In these experiments, GNRs having an AR of 6 and 8, both stabilized with mPEG5000-SH, were utilized. GNR solutions which were prepared at varying dilutions as described in Section 3.2.1 were utilized to have control over the interparticle distance between GNRs. In each experiment, the distance between the GNRs on the surface was determined via Image J analysis of SEM images of the surfaces. Figure 12 shows the representative

SEM images of the surfaces after treatment with the GNRs solutions at three different concentrations. When the images were compared, it could be easily seen that the distance between GNRs on each sample differed. The interparticle distance was the shortest when the GNRs solution applied was the most concentrated (Figure 12). The mean interparticle distance was calculated by measuring the distance of at least 100 GNRs with the surrounding GNRs at different regions of at least three different images of the same sample. Table 5. shows the measured mean interparticle distance and standard error values.

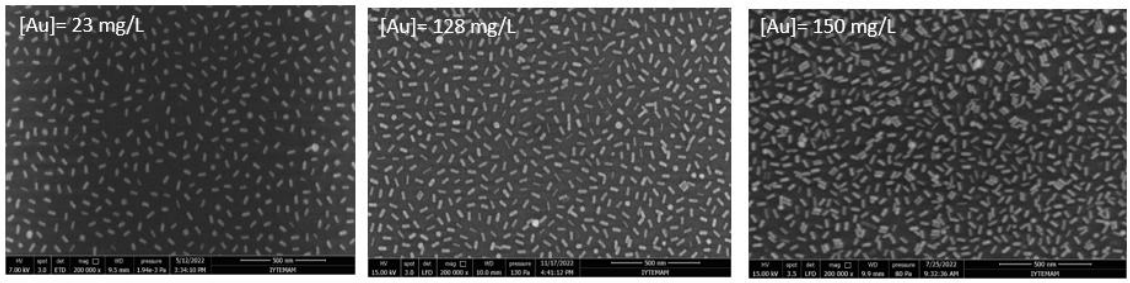

Figure 12. SEM images of the silanized glass surfaces after treatment with GNRs (AR= 6, stabilized with mPEG5000-SH) solutions at three different concentrations. Scale bar is 500 nm. (A) GNR solution 23 mg/L, (B) GNR solution 128 mg/L, (C) GNR solution 150 mg/L.

Table 5. The mean interparticle distance between GNRs on the silanized glass surfaces after treatment with GNR solutions at three different concentrations (GNRs' AR= 6, stabilized with mPEG5000-SH).

Concentration of GNR Solution Used for Surface Functionalization (mg/L)	**Mean Interparticle Distance ± Standard Error (nm)*(calculated via ImageJ analysis of SEM images)**
23	~21±5,3
128	~35±2,8
150	~65±2,5

*Mean of at least 100 GNRs on at least three different SEM images.

The SEM images and subsequent Image J analyses clearly showed that it was possible to control the interparticle distance between the GNRs on the glass surfaces

utilizing GNRs solutions at varying dilutions for functionalization. In summary, glass surfaces decorated with GNRs (having an AR of 6) at three different interparticle distances were successfully prepared to investigate the effect of GNRs' interparticle distance on the LSPR reponse.

4.3.2. Coating Glass Surfaces with GNRs Having Different AR

GNRs were chemically synthesized in this work using the seed- growth method. GNR dimensions and monodispersity can be affected by a number of parameters. Silver nitrate concentration, Au seed amount, seed stability, surfactant concentration, surfactant type, and ionic strength of the growth medium are among these parameters. The size of GNRs can be adjusted with careful regulation of water-based growth conditions. Silver nitrate concentration was employed to adjust the aspect ratio in this investigation, while other growth conditions remained constant. By varying the amount of $AgNO_3$ in the growth solution, GNR samples of varied lengths and approximately constant-diameter spherical end caps were produced, as shown in Table 3 and 4. The longitudinal band of the plasmon was red-shifted by increasing the concentration of silver ions in the growth solution and utilizing CTAB as the surfactant. This red shift caused the longitudinal plasmon peak to shift up to 1200 nm, corresponding to an AR of about 8 (shown in Table 3). GNRs with three different ARs (approx 4, 6 and 8) were utilized to functionalize the glass surfaces to investigate the effect of AR on the LSPR response. The dimensions of these GNRs are presented in Table 4.

At the next step, while keeping the interparticle distance constant (at ~65±2,5 nm) by adjusting the GNR solution concentration, the glass surfaces were coated with GNRs having AR of 4, 6 or 8. The SEM images of these surfaces are presented in Figure 13.

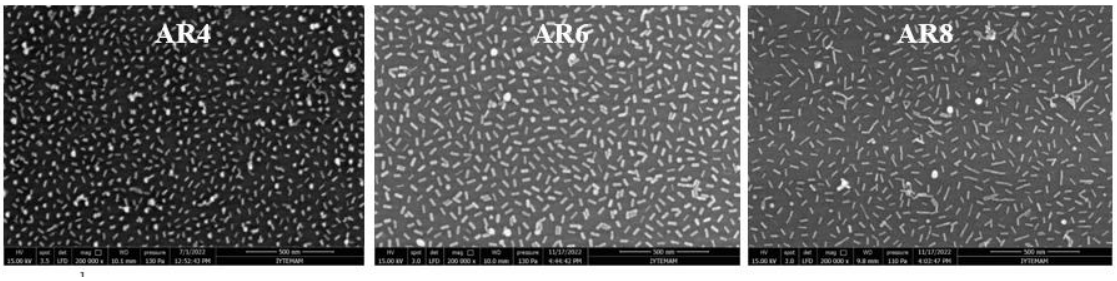

Figure 13. SEM images of glass surfaces coated with GNRs, where the interparticle distance was maintained at approximately 65±2.5 nm. The aspect ratios (AR) of the GNRs were measured to be approximately 4, 6 and 8.

The LSPR spectra of the surfaces decorated with GNRs having different ARs are given in Figure 13. The LSPR spectra clearly proves that the glass surfaces were decorated with GNRs having different ARs since the longitudinal plasmon peak of glass surfaces red-shifts significantly (Figure 14).

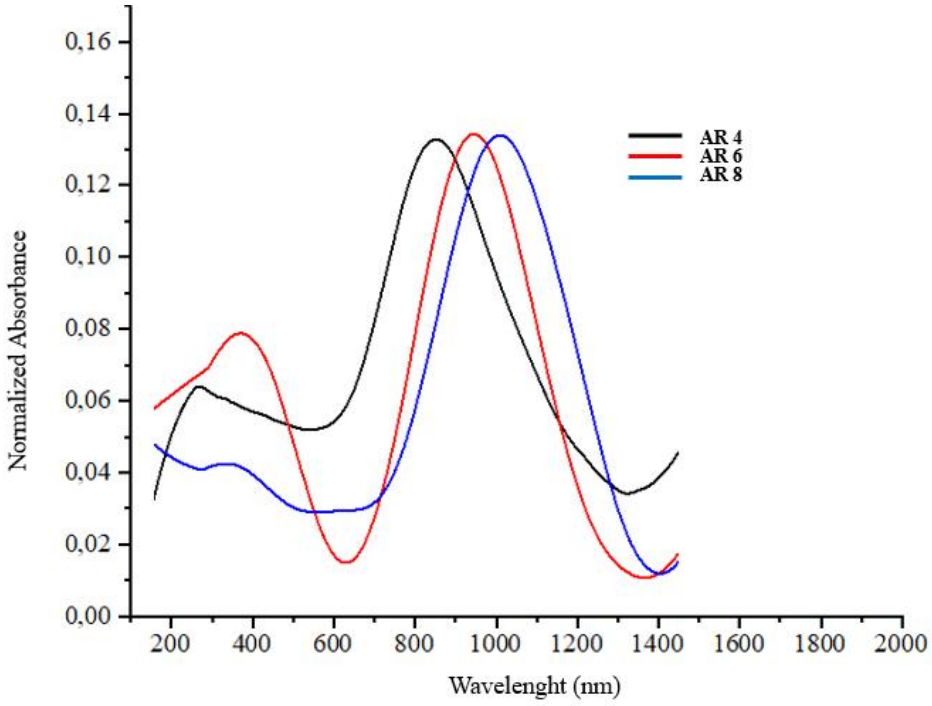

Figure 14. LSPR peaks of surfaces decorated with GNRs having different AR values.

4.4 The Effect of GNRs' Interparticle Distance on the LSPR Response

To investigate the effect of GNRs' interparticle distance and AR on their LSPR response, the GNRs coated glasses were subjected to a mixture of alkanethiols

(alkanethiols) namely 11-mercapto-undecanol and 23-9 mercapto nonyl-3,6,9,12,15,18,21-heptaoxatricosanoic acid for 24 hours and the shift in the longtidunal absorption band after the exposure to alkanethiols and subsequent washing steps was measured using a Vis-NIR spectrometer. Before treating the GNRs coated glass surfaces with alkanethiols, the surfaces were exposed to oxygen plasma to remove the mPEG5000-SH molecules on the GNRs surface and obtain plain gold nanorods on the glass surfaces suitable for attachment of alkanethiols. The efficacy of oxygen plasma in eliminating polyethylene glycol (PEG) without disturbing the GNRs attachment on the glass slides was determined via LSPR and SEM. The decrease in the LSPR spectrum of glass surfaces after oxygen plasma was attributed to the complete removal of PEG molecules in GNRs (Figure 15). Glass surfaces bearing bare GNRs after plasma treatment were then incubated with alkane thiol solution.

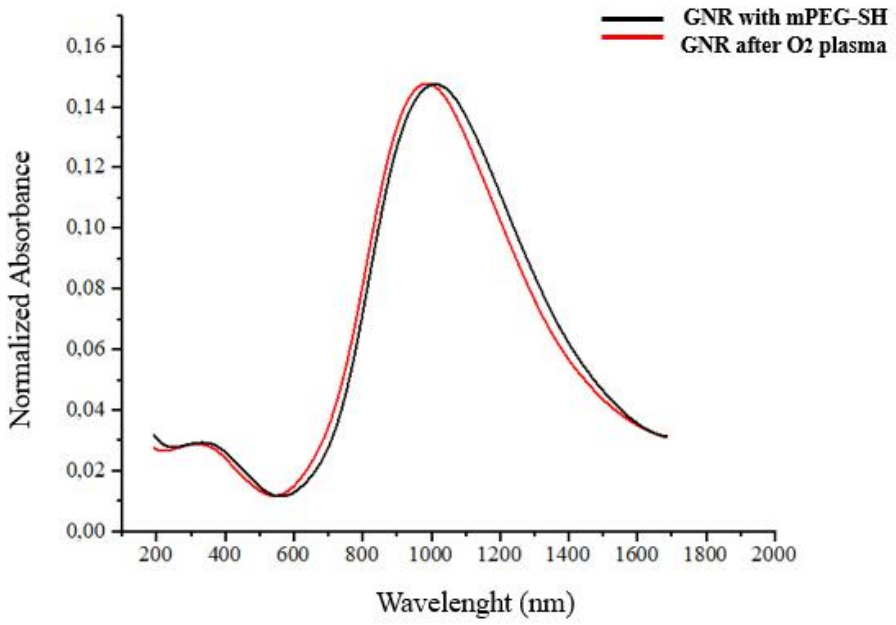

Figure 15. LSPR spectra of glass surfaces before and after oxygen plasma

First, surfaces with varying interparticle distances between GNRs of a constant AR of 6 were exposed to alkane thiols and the shift in the longitudinal plasmon band was observed via a VIS-NIR spectrometer. Figure 16 shows representative LSPR spectra of surfaces with mean interparticle distances of 65±2.5 nm, 35±2.8 nm, and 20±5,3 nm before and after treatment with alkanetiols.

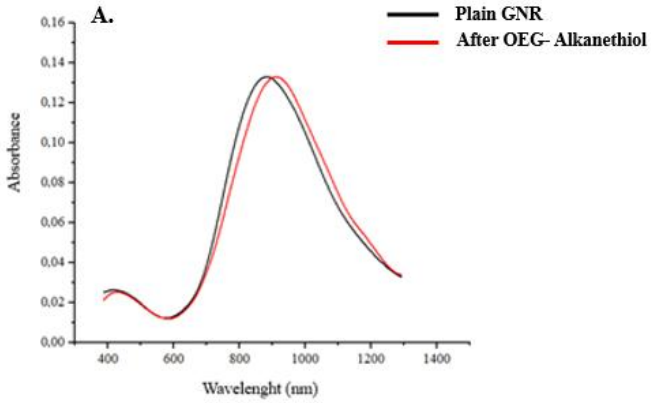
A.
Plain GNR
After OEG- Alkanethiol
Absorbance
0,16
0,14
0,12
0,10
0,08
0,06
0,04
0,02
0,00
400
600
800
1000
1200
1400
Wavelenght (nm)

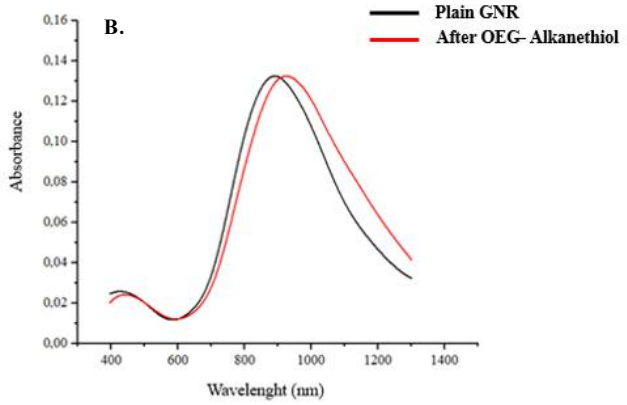
B.
Plain GNR
After OEG- Alkanethiol
Absorbance
0,16
0,14
0,12
0,10
0,08
0,06
0,04
0,02
0,00
400
600
800
1000
1200
1400
Wavelenght (nm)

(cont. on next

Figure 16 (cont.)

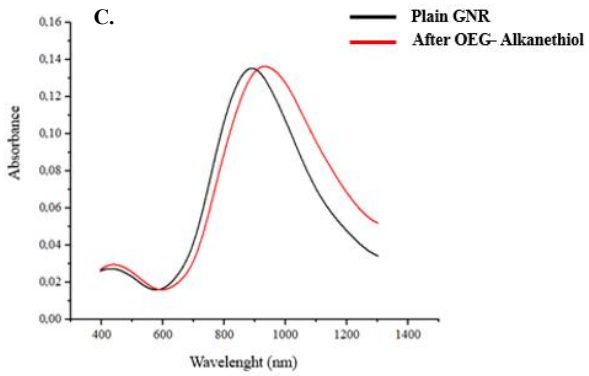

Figure 16. The longitudinal plasmon resonance wavelength of glass surfaces having GNRs (AR=6) with a mean interparticle distance of (A) 20±5,3 nm, (B) 35±2,8 nm, and (C) 65±2,5 nm, before and after treatment with OEG-alkanethiols.

The results can be summarized as follows: As the interparticle distance of the GNRs increases, an increasing trend was observed in the shift of the maximum absorption wavelength upon attachment of alkanethiols to GNRs. LSPR measurements were obtained from five different sensor chips (n=5) for each particular interparticle distance. An average peak shift of 63±3.7 nm was observed for GNRs located with a mean interparticle distance of 65 nm. Similarly, peak shifts of GNRs functionalized surfaces having a mean interparticle distance of 35 nm and 20 nm were found to be 32 nm (±1.8) and 14 nm (±2.2) respectively (Table 6 and Figure 17).

Table 6. The effect of interparticle distance on the shift in λmax after alkanethiol attachment

Aspect Ratio (nm)	**The Interparticle Distance±Standard Error (nm)**	**Shift in λmax After Alkanethiol Attachment (nm)**
6	~65±2,5	63±3,7
6	~35±2,8	32±1,8
6	~20±5,3	14±2,2
8	~65±4,0	64±3,1
8	~35±4,9	54±3,7

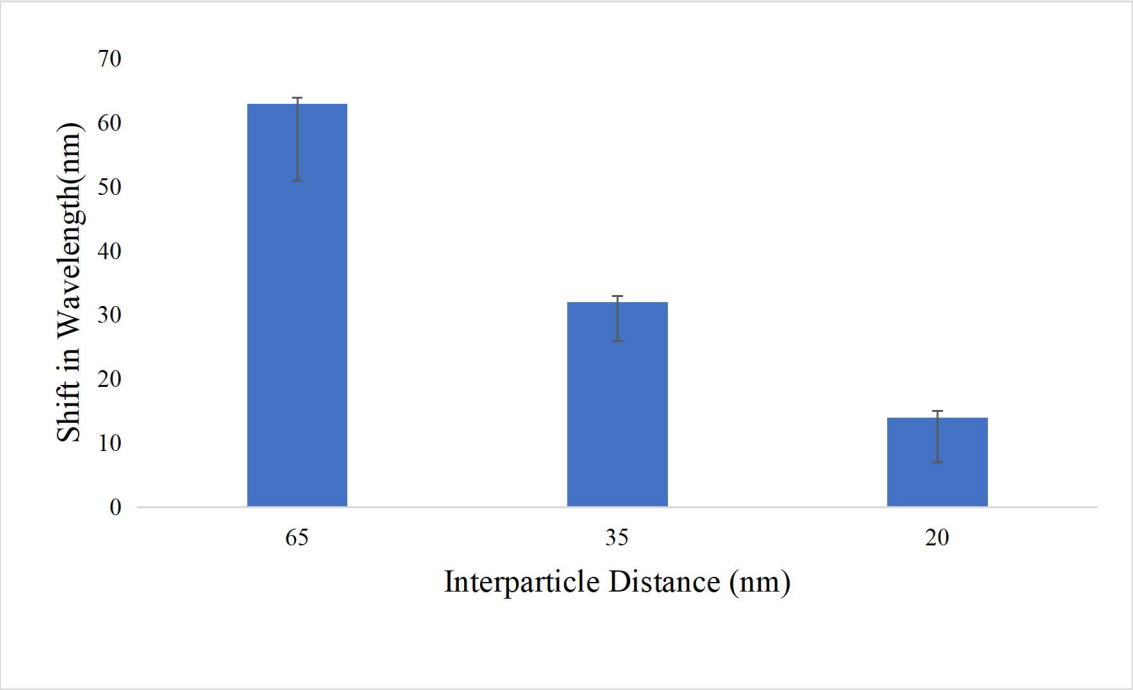

Figure 17. LSPR peak mean shift after alkanethiol attachment onto glass surfaces functionalized with GNRs having an AR of 6 at varying interparticle distance (n=5).

The results show that the distance between the GNRs has a significant effect on the LSPR resonance wavelength. The plasmonic response of GNRs was reduced at close distances. When the distance between the GNRs is large, they cause higher maximum wavelength shift in the LSPR spectrum.

In the event of uniform dispersion at larger interparticle distance, it is anticipated that each individual nanorod will exhibit a distinctive localized surface plasmon resonance (LSPR) spectrum as a result of insignificant inter-nanorod interaction. Typically, the spectra exhibit a narrow profile and display peaks at specific wavelengths. It is a well-established phenomenon that individual nanorods demonstrate plasmon resonance and retain spectral sharpness when arranged in a regular distribution.

The principal factors contributing to the reduction in LSPR shift as proximity is increased may include the increased interparticle interactions, decreased nanorod-light interactions and enhanced steric hindrance against analyte binding. The proximity of closely positioned gold nanorods leads to an escalation in electrical interactions. The plasmon resonance frequencies of the nanorods can be influenced by these interactions. The phenomenon of energy transfers between the surface plasmon polaritons of

nanorods can be attributed to electrical interactions, thereby influencing the shift in LSPR. The interactions between the nanorods result in a reduction in the frequency shift, as the plasmon resonance frequencies of the nanorods become more closely aligned. Furthermore, the reduction of LSPR shift can also be attributed to the enhanced plasmonic coupling between converging nanorods. Hence, the convergence of nanorods and the subsequent increase in their interactions can lead to a decrease in the shift of localized surface plasmon resonance (LSPR) and impose constraints on the extent of spectral variation.

The interparticle distance between GNRs with a higher AR (=8) appeared to have less effect on the LSPR response in the studied range (Figure 18). A long rod (AR8) can produce a stronger LSPR signal and the closer it gets, the less affected the plasmon resonance. The dimensions of a gold nanorod affect the plasmon resonance frequency. A longer nanorod tends to have a lower plasmon resonance frequency. Therefore, the plasmon resonance frequency of AR8 may be lower compared to AR6. As the distance between the nanorods decreases, the electrical interactions increase and can affect the plasmon resonance frequency. However, a long nanorod (AR8) can better tolerate the effect of these interactions as it produces a stronger plasmon resonance signal. In this case, the convergence of AR8s may result in less LSPR shift. Long nanorods (AR8) may have a larger polarization moment, which may contribute to less influencing of plasmon resonances as a result of convergence. For these reasons, a long rod (AR8) is likely to produce stronger LSPR signal and less affected plasmon resonance in case of convergence.

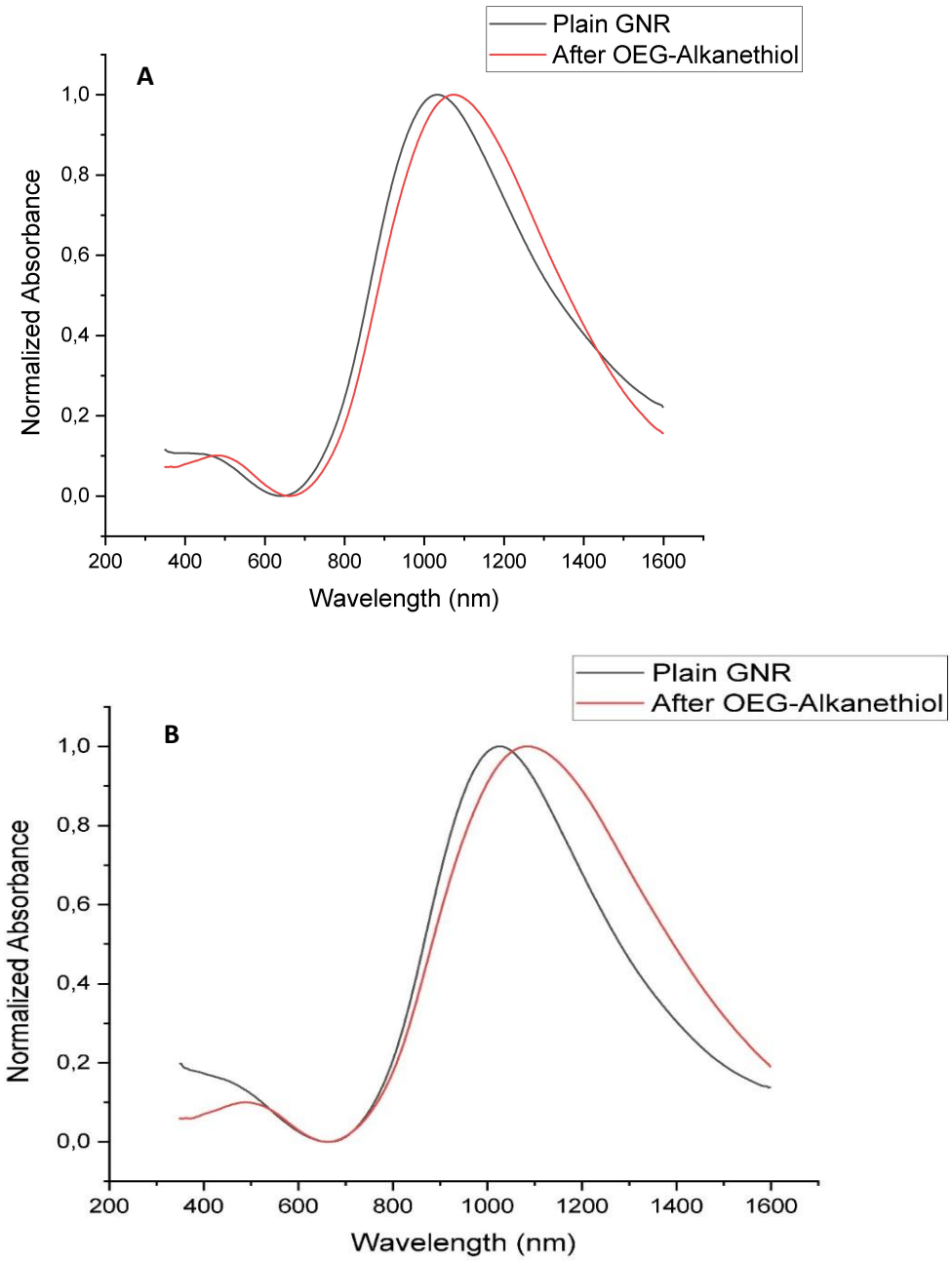

Figure 18. The longitudinal plasmon resonance wavelength of glass surfaces having GNRs (AR=8) with a mean interparticle distance of (A) 35±2,8 nm and (B) 65±2,5 nm, before and after treatment with OEG-alkanethiols.

These results play an important role in designing and optimizing the performance of GNR-based LSPR sensors. Controlling the distance between GNRs can affect the sensitivity and detection limits of the sensor. Therefore, understanding the effect of distance between GNRs on LSPR may contribute to the development of more effective and sensitive sensors.

4.5. The Effect of GNRs' Aspect Ratio on the LSPR Response

Finally, the LSPR response of the glass surfaces functionalized with GNRs with an AR of 4, 6 and 8 was measured after treatment of the surfaces with alkanethiols. Experiments were performed using surfaces functionalized with GNRs at a fixed interparticle distance (65 nm). Measurements were obtained from five different sensor chips (n=5) for each particular AR.

Table 7 summarizes the results obtained. GNRs with AR 4 showed a lower peak shift compared to GNRs with AR 6 and 8. An average peak shift of 16±3 nm was observed for GNRs with an AR of 4 while the peak shift was 63±3,7 nm and 64±3,1 nm, for GNRs having an AR of 6 and 8, respectively (Table 7 and Figure 19).

The results showed that as the AR of the GNRs increased, the LSPR peak shifts also showed a corresponding trend (Table 7). As longer nanorods exhibit larger, surface area, this surface area creates larger vibration of free electrons, leading to increased shift. These rods also exhibit larger surface area for binding analytes and hence may bind to higher number of molecules. In conclusion, the AR of GNRs played an important role in LSPR response of the chips. As the AR increases, the LSPR peak red-shifts become more significant. This could improve the ability of various biosensor applications to detect target analytes with higher sensitivity.

Table 7. The effect of the particle aspect ratio the shift in λmax upon alkanethiol binding.

Aspect Ratio (nm)	**Shift in λ_{max} After Alkanethiol Attachment (nm)**
4	16±3,0
6	63±3,7
8	64±3,1

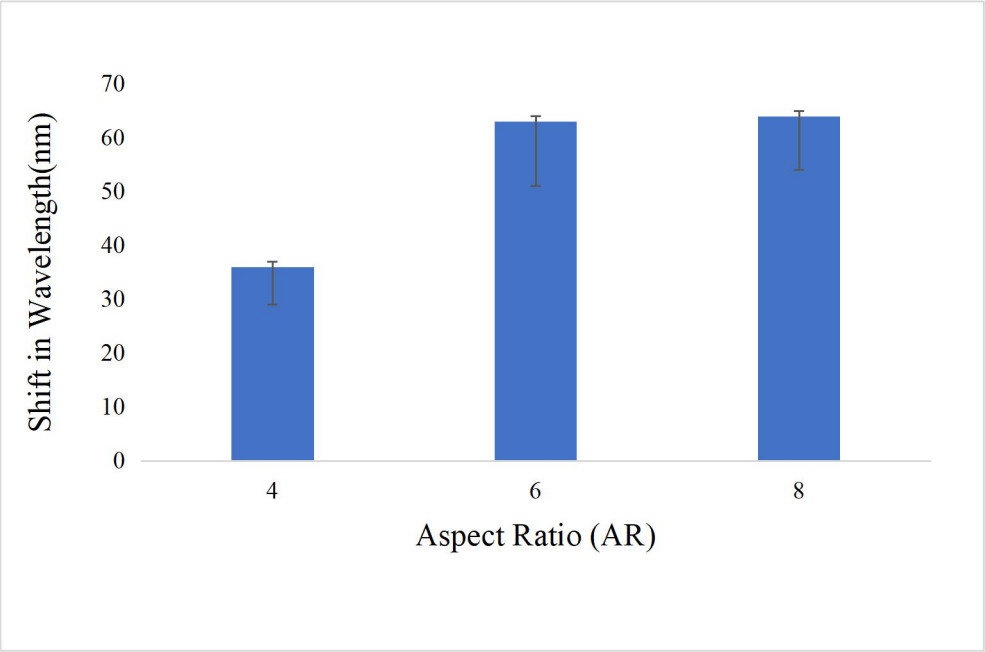

Figure 19. LSPR peak mean shifts after alkanethiol attachment onto glass surfaces functionalized with GNRs having varying aspect ratios (ARs) at a fixed interparticle distance of 65 nm (n=5).

CHAPTER 5

CONCLUSION

GNRs have exceptional optical properties, making them excellent for use in sensors and biosensors. One of the key advantages of GNRs is their high sensitivity to changes in the refractive index of their surroundings. The LSPR phenomenon, in which incident light interacts with the GNRs' collective oscillation of conduction electrons, is what causes this sensitivity. The size, shape, and aspect ratio of GNRs are generally well-known to have the greatest influence on their responsiveness to changes in refractive index. These parameters govern the LSPR's resonance frequency as well as how it responds to local changes in refractive index. By understanding the refractive index sensitivity of GNRs and modifying their shape, size, and aspect ratio, it is feasible to improve the sensitivity and accuracy of LSPR-based sensors.

The aim of this study is to investigate the impact of the aspect ratio and the interparticle distance of GNRs on the localized surface plasmon resonance (LSPR) response of GNRs decorated glass sensor chips. The results from our experiments are summarized below. First, we examined the effect of $AgNO_3$ concentration on the size of GNRs. It was observed that increasing $AgNO_3$ concentration resulted in longer GNRs and a red shift in the longitudinal plasmon peak wavelength. This finding confirms that $AgNO_3$ plays a crucial role in controlling the size and optical properties of GNRs. GNRs with an aspect ratio (AR) of 4, 6 and 8 were obtained.

Poly(ethylene glycol) (mPEG-SH) molecules were used to replace CTAB on the surface of GNRs and keep them stable in aqueous solution. This ligand exchange was confirmed as a change in the wavelength of the maximum absorption in the LSPR spectrum of GNRs. Next, we investigated the effect of the stabilizer molecule type and molecular weight on the distribution of GNRs on the silanized glass surface. For this purpose, GNRs stabilized with CTAB, $mPEG_{2000}$-SH or $mPEG_{5000}$-SH were used to coat glass surfaces. It was found that the APTES modified glass surfaces cannot be coated with CTAB stabilized GNRs. Moreover, using GNRs stabilized with higher molecular weight PEG resulted in a more homogeneous distribution of GNRs on the glass surface. This homogeneous distribution is essential to obtain a consistent and reliable sensor response. The interparticle distance between GNRs on the glass surface was

successfully controlled by simply concentrating or diluting the GNR solution used for coating the glass surfaces. The surfaces were coated with GNRs having a fixed AR at an average interparticle distance of 65±2,5 nm, 35±2,8 nm and 21±5,3 nm (n= 5). It was observed that the LSPR peak shifts decreased upon binding of analytes as the distance between GNRs decreased. This might be attributed to the plasmonic coupling between adjacent GNRs and/or decreased quantity of bound ligands. On the other hand, the AR of GNRs on the glass surface, has also a significant influence on their plasmonic behavior. As the AR decreased, the LSPR response of the GNRs shifted blue. This was attributed to the larger vibration of free electrons in total, and possibly higher quantity of bound molecules, leading to more significant shifts.

In conclusion, this thesis study demonstrates how the LSPR-response of GNR coated glass sensor chips relates to the aspect ratio of GNRs and the interparticle distance. Designing biosensors with increased sensitivity and specificity for the detection of target analytes is attainable by comprehending and improving these factors. These results may contribute to future research to improve the potential of LSPR-based biosensors for diverse biomedical and diagnostic applications.

REFERENCES

Ahmadivand, A., & Pala, N. (2015). Plasmon resonance hybridization in self- assembled copper nanoparticle clusters: efficient and precise localization of surface plasmon resonance (LSPR) sensing based on Fano resonances. *Applied Spectroscopy*, *69*(2), 277-286.

Alhadrami, H. A. (2018). Biosensors: Classifications, medical applications, and future prospective. *Biotechnology and applied biochemistry*, *65*(3), 497-508.

Ameer, F. S. *et al*. Tuning localized surface plasmon resonance wavelengths of silver nanoparticles by mechanical deformation. *J. Phys. Chem. A* **120**, 20886–20895 (2016).

Arghir, I., Delport, F., Spasic, D. & Lammertyn, J. Smart design of fiber optic surfaces for improved plasmonic biosensing. *N. Biotechnol.* **32**, 473–484 (2015).

Bogliotti, N., Oberleitner, B., Di-Cicco, A., Schmidt, F., Florent, J. C., & Semetey, V. (2011). Optimizing the formation of biocompatible gold nanorods for cancer research: functionalization, stabilization and purification. *Journal of colloid and interface science*, *357*(1), 75-81.

Burrows, N. D., Lin, W., Hinman, J. G., Dennison, J. M., Vartanian, A. M., Abadeer, N. S., ... & Murphy, C. J. (2016). Surface chemistry of gold nanorods. *Langmuir*, *32*(39), 9905-9921.

Campbell, D. P. (2008). Interferometric biosensors. In *Principles of bacterial detection: biosensors, recognition receptors and microsystems* (pp. 169-211). Springer, New York, NY.

Cao, J., Sun, T., & Grattan, K. T. (2012, October). Development of gold nanorod-based localized surface plasmon resonance optical fiber biosensor. In OFS2012 22nd International Conference on Optical Fiber Sensors (Vol. 8421, pp. 369-372). SPIE.

Cao, J., Sun, T., & Grattan, K. T. (2014). Gold nanorod-based localized surface plasmon resonance biosensors: A review. *Sensors and actuators B: Chemical*, *195*, 332-351.

Chegel, V., Rachkov, O., Lopatynskyi, A., Ishihara, S., Yanchuk, I., Nemoto, Y., ... & Ariga, K. (2012). Gold nanoparticles aggregation: drastic effect of cooperative functionalities in a single molecular conjugate. *The Journal of Physical Chemistry C*, *116*(4), 2683-2690.

Chen, C., & Wang, J. (2020). Optical biosensors: An exhaustive and comprehensive review. *Analyst*, *145*(5), 1605-1628.

Chen, H. (2013). L. shao, Q. Li and J. Wang. *Chem. Soc. Rev*, *42*, 2679-2724.

Chen, H., Kou, X., Yang, Z., Ni, W., & Wang, J. (2008). Shape-and size-dependent refractive index sensitivity of gold nanoparticles. *Langmuir*, *24*(10), 5233-5237.

Chen, H., Shao, L., Li, Q., & Wang, J. (2013). Gold nanorods and their plasmonic properties. *Chemical Society Reviews*, *42*(7), 2679-2724.

Chirea, M., Cruz, A., Pereira, C. M., & Silva, A. F. (2009). Size-dependent electrochemical properties of gold nanorods. *The Journal of Physical Chemistry C*, *113*(30), 13077-13087.

Christian, T. R., Frank, P. A., & Houston, B. H. (1994, May). Real-time analog and digital demodulator for interferometric fiber optic sensors. In *Smart Structures and Materials 1994: Smart Sensing, Processing, and Instrumentation* (Vol. 2191, pp. 324-336). SPIE.

David, C., Guillot, N., Shen, H., Toury, T., & de la Chapelle, M. L. (2010). SERS detection of biomolecules using lithographed nanoparticles towards a reproducible SERS biosensor. *Nanotechnology*, *21*(47), 475501.

Drobek, T., Spencer, N. D., & Heuberger, M. (2005). Compressing PEG brushes. *Macromolecules*, *38*(12), 5254-5259.

Fu, B., Sun, J., Cheng, Y., Ouyang, H., Compagnini, G., Yin, P., ... & Zhang, H. (2021). Recent Progress on Metal-Based Nanomaterials: Fabrications, Optical Properties, and Applications in Ultrafast Photonics. *Advanced Functional Materials*, *31*(49), 2107363.

Goode, J. A., Rushworth, J. V. H., & Millner, P. A. (2015). Biosensor regeneration: a review of common techniques and outcomes. *Langmuir*, *31*(23), 6267-6276.

Gorbunova, M., Apyari, V., Dmitrienko, S., & Zolotov, Y. (2020). Gold nanorods and their nanocomposites: Synthesis and recent applications in analytical chemistry. *TrAC Trends in Analytical Chemistry*, *130*, 115974.

Gu, X., Timchenko, V., Heng Yeoh, G., Dombrovsky, L., & Taylor, R. (2018). The effect of gold nanorods clustering on near-infrared radiation absorption. *Applied Sciences*, *8*(7), 1132.

Jackson, S. R., McBride, J. R., Rosenthal, S. J., & Wright, D. W. (2014). Where's the silver? Imaging trace silver coverage on the surface of gold nanorods. *Journal of the American Chemical society*, *136*(14), 5261-5263.

Jaeschke, C., Glöckler, J., El Azizi, O., Gonzalez, O., Padilla, M., Mitrovics, J., & Mizaikoff, B. (2019). An innovative modular eNose system based on a unique combination of analog and digital metal oxide sensors. *ACS sensors*, *4*(9), 2277-2281.

Jana, N. R., Gearheart, L., & Murphy, C. J. (2001). Wet chemical synthesis of high aspect ratio cylindrical gold nanorods. *The Journal of Physical Chemistry B*, *105*(19), 4065-4067.

Jeong, H. H. *et al*. Real-time label-free immunoassay of interferon-gamma and prostate-specific antigen using a fiber-optic localized surface plasmon resonance sensor. *Biosens. Bioelectron.* **39**, 346–351 (2013).

Jeong, H. H., Erdene, N., Park, J. H., Jeong, D. H., & Lee, S. K. (2012). Analysis of fiber-optic localized surface plasmon resonance sensor by controlling formation of gold nanoparticles and its bio-application. *Journal of nanoscience and nanotechnology*, *12*(10), 7815-7821.

Jiang, L., Tang, Y., Liow, C., Wu, J., Sun, Y., Jiang, Y., ... & Chen, X. (2013). Synthesis of Fivefold Stellate Polyhedral Gold Nanoparticles with {110}-Facets via a Seed-Mediated Growth Method. *Small*, *9*(5), 705-710.

Kadkhodazadeh, S., Christensen, T., Beleggia, M., Mortensen, N. A., & Wagner, J. B. (2017). The substrate effect in electron energy-loss spectroscopy of localized surface plasmons in gold and silver nanoparticles. *ACS photonics*, *4*(2), 251-261.

Kahraman, M., Mullen, E. R., Korkmaz, A., & Wachsmann-Hogiu, S. (2017). Fundamentals and applications of SERS-based bioanalytical sensing. *Nanophotonics*, *6*(5), 831-852.

Kaur, B., Kumar, S., & Kaushik, B. K. (2022). Recent advancements in optical biosensors for cancer detection. *Biosensors and Bioelectronics*, *197*, 113805.

Kim, H. M., Nam, K. T., Lee, S. K., & Park, J. H. (2018). Fabrication and measurement of microtip-array-based LSPR sensor using bundle fiber. *Sensors and Actuators A: Physical*, *271*, 146-152.

Kim, H. M., Park, J. H., & Lee, S. K. (2019). Fiber optic sensor based on ZnO nanowires decorated by Au nanoparticles for improved plasmonic biosensor. *Scientific reports*, *9*(1), 1-9.

Lai, Z., Tan, J., Wan, R., Tan, J., Zhang, Z., Hu, Z., ... & Zhao, Y. (2017). An 'activatable'aptamer-based fluorescence probe for the detection of HepG2 cells. *Oncology reports*, *37*(5), 2688-2694.

Langhammer, C., Zorić, I., Kasemo, B. & Clemens, B. M. Hydrogen storage in Pd nanodisks characterized with a novel nanoplasmonic sensing scheme. *Nano Lett.* **7**, 3122–3127 (2007).

Larson, S., Yang, Z., & Zhao, Y. (2019). Improving LSPR sensing performance using multilayered composition graded Ag–Cu nanotriangle arrays. *Chemical Communications*, *55*(9), 1342-1344.

Lee, B., Park, J. H., Byun, J. Y., Kim, J. H. & Kim, M. G. An optical fiber-based LSPR aptasensor for simple and rapid *in-situ* detection of ochratoxin A. *Biosens. Bioelectron.* **102**, 504–509 (2018).

Liao, S., Yue, W., Cai, S., Tang, Q., Lu, W., Huang, L., ... & Liao, J. (2021). Improvement of gold nanorods in photothermal therapy: Recent progress and perspective. *Frontiers in Pharmacology*, 781.

Lin, D. Z., Chuang, P. C., Liao, P. C., Chen, J. P., & Chen, Y. F. (2016). Increasing the spectral shifts in LSPR biosensing using DNA-functionalized gold nanorods in a competitive assay format for the detection of interferon-γ. *Biosensors and Bioelectronics*, *81*, 221-228.

Lodewijks, K., Van Roy, W., Borghs, G., Lagae, L., & Van Dorpe, P. (2012). Boosting the figure-of-merit of LSPR-based refractive index sensing by phase-sensitive measurements. *Nano letters*, *12*(3), 1655-1659.

Lohse, S. E., & Murphy, C. J. (2013). The quest for shape control: a history of gold nanorod synthesis. *Chemistry of Materials*, *25*(8), 1250-1261.

Lowe, C. R., Davis, F., Collyer, S. D., Higson, S. P., Newman, J. D., Turner, A. P., & Marks, R. S. (2007). Handbook of biosensors and biochips. *Development*, *41*, 18.

Luong, J. H., Male, K. B., & Glennon, J. D. (2008). Biosensor technology: technology push versus market pull. *Biotechnology advances*, *26*(5), 492-500.

Maier, S. A. (2007). Plasmonics: fundamentals and applications (Vol. 1, p. 245). New York: springer.

Manohar, S., Ungureanu, C., & Van Leeuwen, T. G. (2011). Gold nanorods as molecular contrast agents in photoacoustic imaging: the promises and the caveats. *Contrast media & molecular imaging*, *6*(5), 389-400.

Manzano, M., Vizzini, P., Jia, K., Adam, P. M., & Ionescu, R. E. (2016). Development of localized surface plasmon resonance biosensors for the detection of Brettanomyces bruxellensis in wine. *Sensors and Actuators B: Chemical*, *223*, 295-300.

Mishra, Y. K. & Adelung, R. ZnO tetrapod materials for functional applications. *Mater. Today* **21**, 631–651 (2018)

Newman, J. D., & Setford, S. J. (2006). Enzymatic biosensors. *Molecular biotechnology*, *32*(3), 249-268.

Nikoobakht, B., & El-Sayed, M. A. (2003). Preparation and growth mechanism of gold nanorods (NRs) using seed-mediated growth method. *Chemistry of Materials*, *15*(10), 1957-1962.

Nikoobakht, B., & El-Sayed, M. A. (2003). Preparation and growth mechanism of gold nanorods (NRs) using seed-mediated growth method. *Chemistry of Materials*, *15*(10), 1957-1962.

Perumal, V., & Hashim, U. (2014). Advances in biosensors: Principle, architecture and applications. *Journal of applied biomedicine*, *12*(1), 1-15.

Salavatov, N. A., Dement'eva, O. V., Mikhailichenko, A. I., & Rudoy, V. M. (2018). Some aspects of seedless synthesis of gold nanorods. *Colloid Journal*, *80*(5), 541-549.

Sassolas, A., Blum, L. J., & Leca-Bouvier, B. D. (2012). Immobilization strategies to develop enzymatic biosensors. *Biotechnology advances*, *30*(3), 489-511.

Scarabelli, L., Sánchez-Iglesias, A., Pérez-Juste, J., & Liz-Marzán, L. M. (2015). A "tips and tricks" practical guide to the synthesis of gold nanorods. *The journal of physical chemistry letters*, *6*(21), 4270-4279.

Sivakumar, S. A., Karthikeyan, S., Tephila, M. B., Ganesh, R. S., Kumar, R. S., & Shankar, B. M. (2020). Comparitive analysis of shift register designs for successive approximation analog to digital converters. *International Journal of Advanced Science and Technology*, *29*(8), 2254-2260.

Song, M., Lin, X., Peng, Z., Xu, S., Jin, L., Zheng, X., & Luo, H. (2021). Materials and methods of biosensor interfaces with stability. Frontiers in Materials, 7, 583739.

Söylemez, C. (2020). *Design of localized surface plasmon resonance (LSPR) based biosensor for detecting a potential cancer biomarker* (Doctoral dissertation, Izmir Institute of Technology (Turkey)).

Taykoz, D. (2020). *Development of a Plasmonic Biosensor for Detection of Exosomes* (Doctoral dissertation, Izmir Institute of Technology (Turkey)).

Thevenot, D. R., Toth, K., Durst, R. A., & Wilson, G. S. (1999). Electrochemical biosensors: recommended definitions and classification. *Pure and applied chemistry*, *71*(12), 2333-2348.

Toderas, F., Iosin, M., & Astilean, S. (2009). Luminescence properties of gold nanorods. *Nuclear Instruments and Methods in Physics Research Section B: Beam Interactions with Materials and Atoms*, *267*(2), 400-402.

Tong, W., Walsh, M. J., Mulvaney, P., Etheridge, J., & Funston, A. M. (2017). Control of symmetry breaking size and aspect ratio in gold nanorods: underlying role of silver nitrate. *The Journal of Physical Chemistry C*, *121*(6), 3549-3559.

Turner, A. P. (2013). Biosensors: sense and sensibility. *Chemical Society Reviews*, *42*(8), 3184-3196.

Unser, S., Bruzas, I., He, J., & Sagle, L. (2015). Localized surface plasmon resonance biosensing: current challenges and approaches. *Sensors*, *15*(7), 15684-15716.

Vafapour, Z., Keshavarz, A., & Ghahraloud, H. (2020). The potential of terahertz sensing for cancer diagnosis. *Heliyon*, *6*(12), e05623.

Wang, S., Li, W., Chang, K., Liu, J., Guo, Q., Sun, H., ... & Hu, J. (2017). Localized surface plasmon resonance-based abscisic acid biosensor using aptamer-functionalized gold nanoparticles. *PloS one*, *12*(9), e0185530.

Wang, S., Sun, X., Ding, M., Peng, G., Qi, Y., Wang, Y., & Ren, J. (2018). The investigation of an LSPR refractive index sensor based on periodic gold nanorings array. *Journal of Physics D: Applied Physics*, *51*(4), 045101.

Wu, W., Wang, L., Yang, Y., Du, W., Ji, W., Fang, Z., ... & Li, L. (2022). Optical flexible biosensors: From detection principles to biomedical applications. *Biosensors and Bioelectronics*, 114328.

Zhang, Q., Jing, H., Li, G.G., Lin, Y., Blom, D.A., and Wang, H., Chem. Mater., 2016, vol. 28, p. 2728.

Zhao, V. X. T., Wong, T. I., Zheng, X. T., Tan, Y. N., & Zhou, X. (2020). Colorimetric biosensors for point-of-care virus detections. *Materials science for energy technologies*, *3*, 237-249.

Zhu, J., Yong, K. T., Roy, I., Hu, R., Ding, H., Zhao, L., ... & Prasad, P. N. (2010). Additive controlled synthesis of gold nanorods (GNRs) for two-photon luminescence imaging of cancer cells. *Nanotechnology*, *21*(28), 285106.